NACA RM E53C18

RESEARCH MEMORANDUM

A DESIGN AND PERFORMANCE STUDY OF THE NUCLEAR DIRECT-AIR-CYCLE SUPERSONIC AIRPLANE, INCLUDING THE EFFECTS OF OPERATING TEMPERATURES AND FUEL PLATE MATERIAL AND THICKNESS

By S. V. Manson and William W. Wachtl

Lewis Flight Propulsion Laboratory
Cleveland, Ohio

NATIONAL ADVISORY COMMITTEE FOR AERONAUTICS

OR0102668

WASHINGTON

K3568

JUN 26 1953

NATIONAL ADVISORY COMMITTEE FOR AERONAUTICS

RESEARCH MEMORANDUM

A DESIGN AND PERFORMANCE STUDY OF THE NUCLEAR DIRECT-AIR-CYCLE SUPERSONIC AIRPLANE, INCLUDING THE EFFECTS OF OPERATING TEMPERATURES AND FUEL PLATE MATERIAL AND THICKNESS

By S. V. Manson and William W. Wachtl

SUMMARY

This report presents a study of the effects of high reactor and cycle temperatures, and the effect of thickness of high-temperature fuel element materials, on the feasibility of the nuclear-powered direct-air-cycle aircraft for flight at Mach number of 1.5 at an altitude of 35,000 feet. Reactor fuel temperatures from 2060° to 2960° R, turbine-inlet temperatures to 2600° R, and reactor fuel plate thicknesses of 0.07 and 0.01 inch were covered in this study. The feasibility is expressed in terms of the airplane gross weight and the reactor dimensions required to attain the desired flight performance. The shield thickness and composition were based on a design that allows a crew radiation dosage of one Roentgen per hour.

As part of the study, detailed attention was paid to the internal flow system, component arrangement and weights, external aerodynamics, and, for cases of interest, the reactor fuel-plate thermal stresses and shock. Bases for design and the analytical methods employed for calculation are indicated in detail.

On the basis of the assumptions of the report the airplane gross weights and reactor dimensions required to attain the flight Mach number of 1.5 at 35,000 feet are:

Case	Fuel Plate			Turbine-inlet temperature, °R	Airplane gross weight, lb	Reactor		
	Material	Temperature, °R	Thickness, in.			Heat release, Btu/sec	Diameter, ft	Length, ft
I	Metal	2060	0.01	1900	535,000	520,000	9.5	3.25
IIA	Ceramic	2660	.07	2000	480,500	504,000	8.5	3.14
IIB	Ceramic	2660	.01	2000	442,000	449,000	8.0	3.28
IIIB	Ceramic	2960	.07	2600	318,000	370,500	5.5	4.05
IIIA	Ceramic	2960	.01	2600	291,500	332,000	5.0	4.10

The compressor pressure ratios at which these results were obtained, together with results at other cycle operating conditions, and a discussion of thermal stresses, are presented in the body of this report.

INTRODUCTION

For supersonic flight with the nuclear direct-air-cycle aircraft, a high reactor fuel-element temperature is desirable. A high fuel temperature may require the use of nonmetallic materials, such as ceramals, ceramics, and intermetallics. It may not be possible to fabricate these materials into plates as thin as those possible with metals; hence, some of the advantages of the higher permissible fuel-element temperature may be balanced by the smaller amount of heat-transfer surface that can be installed per unit volume of reactor for these nonmetallic materials. The principal purpose of the present report was, therefore, to explore the effects of thickness and temperature of reactor fuel elements on the feasibility of the direct air cycle for supersonic aircraft, in order to obtain some insight into the desirability of a development program on nonmetallic materials for nuclear reactors.

For the study, flight at 35,000 feet at a Mach number of 1.5 has been specified. In connection with these flight specifications the purposes of the present report are:

(1) to determine the reactor dimensions, fuel-plate thermal stresses, and aircraft gross weight, at the conditions defined as cases I, II, and III, listed in the following table:

Item	Case I	Case II	Case III
Flight Mach number	1.5	1.5	1.5
Altitude, ft	35,000	35,000	35,000
Compressor pressure ratio	15	15	15, 20, 25
Turbine-inlet temperature, $^{\circ}R$	1900	2000	2000, 2300 2600
Reactor fuel element surface temperature, $^{\circ}R$	2060	2660 2960	2960
Fuel element thickness, in.	0.01	0.07 .01	0.01 .07

Case I is representative of a system employing metal fuel elements, and cases II and III represent systems employing ceramic fuel elements.

(2) To arrange the direct-air cycle components in a configuration which would provide small frontal area of the nacelle, and an efficient air flow system, toward achievement of purpose (1).

This study was performed at the NACA Lewis laboratory, during the period February to September 1952.

DESCRIPTION OF SYSTEM

External Configuration

Fuselage. - A schematic view of the airplane is shown in figure 1. The fuselage consists of a conical nose section which houses the crew and maintains a 50-foot separation between the crew shield and the reactor shield; an annular air intake between the cone section and the main body; a cylindrical main body section which houses the reactor, shield, and engines; and a conical boattail section which houses the jet exhaust nozzles.

Shield. - As shown in figure 1, the separated shield system comprises a water shield around the reactor, a lead shadow shield between the reactor shield and the crew compartment, a 50-foot air separation distance between the reactor shield and the crew compartment, and a lead and plastic shield surrounding the crew compartment. This shield arrangement is similar to that shown in reference 1, and allows a crew radiation dosage of one Roentgen per hour.

Engines. - Six engines are assumed located circumferentially about the fuselage center line. Inasmuch as a nonreversing air flow path from the diffuser to jet nozzles was desired, and inasmuch as long hollow shafts and suitable bearings were thought potentially feasible, the compressor and turbine are visualized as straddling the shielded reactor (fig. 1). Pending radiation damage studies, the shafts are visualized as penetrating the water shield with provisions for water flow axially through the shaft interiors. This arrangement, which is shown in figure 1 and described more in detail in appendix B, was believed to lead to minimum weight of the shield and to minimum fuselage frontal area, ducting, and air pressure drop.

Internal Flow System

Air flow path. - The internal air flow path between compressor outlet and turbine-inlet is shown in figure 2. The visualized components of the flow path were, in succession, a guide-vaned plenum chamber, an end shield upstream of the reactor, the reactor, an end shield downstream of the reactor, and another vaned plenum chamber. The end shields, sketched in figure 3, were designed to provide four 30° bends

in the path of streaming neutrons; moderate reflection at the reactor ends; good air flow distribution into and out of the reactor; no increase in frontal area relative to the side shield, nor superfluous axial mass; and ease of fabrication. The free flow ratio in the upstream shield was 0.3, and the tube size ranged from 1/4 inch at the lowest air flow to $1\frac{1}{4}$ inch at the highest air flow considered. Because the upstream shield free flow ratio was 0.3, the three straight portions of any one tube could be visualized as offset so that no two straight lengths were in line (fig. 3). The downstream shield free ratio was always greater than 0.3, ranging from 0.4 to 0.5 at the highest air flows of interest. The increase in downstream shield flow area was introduced to provide the same pressure loss as in the upstream shield, with the result that the downstream shield was slightly more transparent to streaming neutrons than the upstream shield. Tube diameters in the downstream shield were assigned the same values as in the upstream shield. The tubes were assumed to be externally insulated, and the space between tubes to be filled by circulating water. The shield-water cooling system was not considered.

Reactor. - Forty-eight percent of the reactor volume was assigned to moderator, structure, and insulating materials; the remaining 52 percent was assumed taken by fuel-bearing material and air-flow space. No detailed reactor surface design was attempted, inasmuch as physical properties of the hypothetical ceramic were unknown, but for calculation an arrangement like that sketched in figure 4 was postulated. Thus, the surface was preliminarily visualized as consisting of platelets in series, touching at front and rear edges to provide a smooth passage, and containing variable fuel content in successive platelets to provide an isothermal surface.

METHODS

Thrust and Drag Determinations

Available thrust. - The available net thrust from the engines was determined from cycle calculations as shown in appendix B, equations (B32) and (B33), based upon the temperatures, pressure ratios, and losses in the system (see appendix A for symbols):

$$(F_n)_{avail} = \left(\frac{F_j}{w_a} - \frac{V_0}{g}\right) w_a \qquad (B32)$$

where

$$\frac{F_j}{w_a} = C_v \sqrt{\frac{2Jc_pT_6}{g}\left[1 - \left(\frac{p_0}{p_6}\right)^{\frac{\gamma-1}{\gamma}}\right]} \qquad (B33)$$

Required thrust. - The design point fuselage and component sizes, weight, and aerodynamic drag were determined as functions of reactor size and air flow by the methods shown in appendix B. From the drag and gross weight calculated, the total required thrust for level flight was determined as follows:

$$(F_n)_{req} = D_w + D_F + D_t \qquad (B1)$$

The wing drag D_w is a function of the airplane gross weight and the wing lift-drag ratio. The tail drag D_t was assumed to be 10 percent of the wing drag. Therefore:

$$(F_n)_{req} = \frac{1.1\ W_g}{(L/D)_w} + D_F \qquad (B12)$$

where the wing lift-drag ratio, which was determined as shown in appendix B to be 8.3, was assumed to be constant for all operating conditions. The components of the fuselage drag D_F are given by equations (B18), (B20), and (B23), and include the drag of the nose section, main body, and boattail. (Sketches of these sections are shown in figs. 5 to 7.) Thus, on adding the component drags,

$$D_F = D_{nose} + D_y + D_z$$

Procedure. - The values of total thrust, $(F_n)_{req}$ and $(F_n)_{avail}$, were calculated for three reactor surface temperatures T_S, four turbine-inlet temperatures T_5, three compressor pressure ratios P_2/P_1, two fuel plate thicknesses ϵ, a range of reactor diameters d_R, and a range of air flows per reactor frontal area w_a/A_R. For each combination of T_S, T_5, P_2/P_1, ϵ, and d_R, both $(F_n)_{avail}$ and $(F_n)_{req}$ were plotted against w_a/A_R, as shown in figure 8. The intersection of the curves of $(F_n)_{avail}$ and $(F_n)_{req}$ determined the minimum air flow w_a/A_R and the thrust necessary to fly the airplane. (Curves of specific thrust, $(F_n)_{avail}/w_a$ and $(F_n)_{req}/w_a$, are also presented, and the information from this plot is discussed in the section "Results and Discussion.") The airplane gross weight W_g, total engine air flow w_a, and reactor heat release Q were then obtained at the determined value

of w_a/A_R, and the values of air pressure drop P_5/P_2 and reactor length corresponding to w_a/A_R were also determined. These values were then plotted against reactor diameter, as shown in figures 9 to 12, thus giving a series of design-point airplanes as a function of reactor size for the range of operating conditions considered.

Heat Transfer

Heat-transfer equations. - The average heat-transfer coefficient in the smooth-passaged reactor was computed by the formula in reference 2

$$\frac{h_{av}d_e}{K_\phi} = \frac{0.034}{(l/d_e)^{0.1}} Pr_\phi^{0.4} Re_\phi^{0.8} \tag{1}$$

It was assumed that at $l/d_e = 50$ the surface was interrupted and the boundary layer started anew; hence the formula becomes:

$$\frac{h_{av}d_e}{K_\phi} = 0.023 Pr_\phi^{0.4} Re_\phi^{0.8} \tag{2}$$

where

$$\left.\begin{aligned} Pr_\phi &\equiv \frac{c_{p,\phi}\mu_\phi}{K_\phi} \\ Re_\phi &\equiv \frac{w_a}{(\alpha A_R)} \frac{d_e}{\mu_\phi} \frac{T_{av}}{T_\phi} \\ T_{av} &\equiv \frac{1}{2}(T_3 + T_4) \\ T_\phi &\equiv \frac{(T_{av} + T_S)}{2} \end{aligned}\right\} \tag{3}$$

Specific heats and viscosities were obtained from reference 3. Conductivities were obtained from reference 4; if used in formula (2), these conductivities result in heat-transfer coefficients that are approximately 10 percent optimistic and hence tend to present the dimensions of the direct-cycle reactor in a slightly favorable light. The relation employed for computing the required surface per reactor frontal area at constant wall temperature was

$$\frac{h_{av}S_R}{w_a c_{p,av}} = \ln\left(\frac{T_S - T_3}{T_S - T_4}\right)$$

in which total temperatures appear because the formula for h_{av} is based on total temperatures; or

$$\frac{S_R}{A_R} = \left(\frac{c_{p,av}}{h_{av}}\right)\left(\frac{w_a}{A_R}\right) \ln\left(\frac{T_S - T_3}{T_S - T_4}\right) \tag{4}$$

Equivalent diameter of reactor flow passage. - In order to use equation (4), a knowledge of the equivalent diameter d_e of the reactor flow passage was necessary, as indicated in equation (2) for the heat-transfer coefficient h_{av}. The equivalent diameter was taken as

$$d_e \equiv \frac{4(\alpha A_R)}{\text{heated perimeter}} = 4\alpha l_R \left(\frac{A_R}{S_R}\right) \tag{5}$$

For a plate of thickness ε inch, the surface-to-volume ratio is

$$\frac{S_R}{v_R} = \frac{24}{\varepsilon}, \frac{ft^2}{ft^3} \tag{6}$$

If the frontal area occupied by air passage plus fuel plate is $0.52\ A_R$, and if the frontal area of the air passage alone is αA_R, the plate volume is

$$v_R = (0.52 - \alpha)(A_R l_R) \tag{7}$$

From equations (6) and (7)

$$\frac{S_R}{A_R} = \frac{24(0.52 - \alpha) l_R}{\varepsilon} \tag{8}$$

On substituting equation (8) into (5),

$$d_e = \frac{\varepsilon}{6}\left(\frac{\alpha}{0.52 - \alpha}\right) \tag{9}$$

(This value of d_e was also used in computing the pressure drop due to friction.)

Reactor surface and length. - From equations (9), (2), and (4), S_R/A_R was obtained; and when a d_R was prescribed, the total reactor heat-transfer surface was determined.

From equations (6) and (7) the reactor length is

$$l_R = \left(\frac{\epsilon}{24}\right)\left(\frac{S_R}{A_R}\right)\left(\frac{1}{0.52 - \alpha}\right) \tag{10}$$

The design procedure consists in prescribing ϵ, α, T_S, T_3, T_4, and w_a/A_R, and using the indicated equations. Calculations were made for ϵ of 0.01 and 0.07 inch; α from 0.36 to 0.51; T_S of 2060°, 2660°, and 2960° R; and T_3 of 1345°, 1465°, and 1565° R corresponding to the assumed P_2/P_1; T_4 of 1900°, 2000°, 2300°, and 2600° R; and w_a/A_R from 15 to 80 pounds per second per square foot.

2659

Pressure Drop

The air flow path shown in figure 2 is characterized by 90° bends in sections AB and ST; sudden contractions in sections BC, IJ, and LM, miter bends in sections DE, FG, NO, and PQ; sudden expansions in sections HI, KL, and RS, and straight ducts of constant flow area in sections CD, EF, GH, JK, MN, OP, and QR. The relations employed to evaluate static pressure changes in the various sections are listed below.

90° bends. - For a suitably vane-guided 90° bend, 20 percent of the local velocity head was assumed lost (ref. 5).

Miter bends. - For two 30° miter bends in series, 25 percent of the local velocity head was assumed lost (ref. 6).

Sudden contraction. - For sudden contraction of a compressible fluid, the following equation was employed:

$$1 - \left(\frac{\rho_d}{\rho_u}\right)^{\gamma-1} = 0.5\,(\gamma-1)\,M_u^2\left[\frac{1}{\left(\alpha\,\frac{\rho_d}{\rho_u}\right)^2} - 1\right] \tag{C13}$$

(The origin of this equation is indicated in appendix C.) This equation was solved graphically for ρ_d/ρ_u, and the downstream static pressure was then computed by the relation

$$\frac{p_d}{p_u} = \left(\frac{\rho_d}{\rho_u}\right)^{\gamma}$$

Vena contracta. - After contraction, the static pressure was charged with the vena contracta loss associated with a slightly rounded entrance, that is, 10 percent of the downstream velocity head (ref. 7).

Subsonic sudden expansion. - For subsonic sudden expansion into a chamber of an axial depth of approximately 4.5 equivalent diameters of the upstream passage, full pressure recovery was assumed (ref. 8) and the following relations were used:

$$\frac{\rho_u}{\rho_d} = \frac{(1+\alpha\gamma M_u^2) - \sqrt{(1+\alpha\gamma M_u^2)^2 - (\gamma+1)(\alpha M_u)^2\left[2+(\gamma-1)M_u^2\right]}}{(\gamma+1)(\alpha M_u)^2} \tag{C11}$$

$$\frac{p_d}{p_u} = 1 + \gamma\alpha M_u^2\left(1 - \alpha\frac{\rho_u}{\rho_d}\right) \tag{C10}$$

(The origin of these equations is indicated in appendix C.)

Straight duct. - For a straight duct of constant flow area, the fluid static pressure was first reduced by 9 percent of the local velocity head to account for the portion of the flow work converted to the kinetic energy of a turbulent velocity profile, and then the passage static pressure drop was computed by addition of the skin friction and the over-all rate of momentum change for a compressible fluid; this procedure fits very well the experimental results of reference 2 in the Reynolds number range of interest in the present study. The skin friction relation is

$$\left.\begin{aligned}
\Delta p_f &= 4\, f_\phi \left(\frac{l_R}{d_e}\right)\left(\frac{G_3^2}{2\rho_{av}g}\,\frac{t_{av}}{t_\phi}\right) \\
\text{where} \\
f_\phi &= \frac{0.046}{\left(\frac{G_3 d_e}{\mu_\phi}\,\frac{t_{av}}{t_\phi}\right)^{0.20}} \\
\rho_{av} &= \frac{\rho_3 + \rho_4}{2} \\
t_{av} &= \frac{t_3 + t_4}{2} \\
t_\phi &= \frac{t_{av} + t_S}{2}
\end{aligned}\right\} \tag{11}$$

The momentum relation is

$$\Delta p_m = \frac{G_3^2}{\rho_3 g}\left(\frac{\rho_3}{\rho_4} - 1\right) \tag{12}$$

The relation

$$\Delta p = \Delta p_f + \Delta p_m \tag{13}$$

was solved graphically for ρ_3/ρ_4. Equations (11) to (13) apply to the reactor and the straight portions of the shield tubes.

Interruption loss. - As indicated in the section "Reactor Heat Transfer," the reactor heating surface was assumed to be interrupted at each l/d_e of 50. These interruptions were accounted for by charging the inlet pressure with as many times the velocity profile energy conversion (as discussed under straight duct flow) as there were interruptions.

Thermal Stress

The thermal stresses were evaluated by the method of reference 9, as discussed in appendix D.

RESULTS AND DISCUSSION

The selected components and their arrangements have been described under "System" and in figures 1 to 7. The results of performance calculations are presented in figures 9 to 23. As stated in the "Introduction," the calculations were made for cases I, II, and III defined as follows:

Variable	Case I	Case II	Case III
Flight Mach number, M_0	1.5	1.5	1.5
Altitude, ft	35,000	35,000	35,000
Compressor pressure ratio, P_2/P_1	15	15	15, 20, 25
Turbine-inlet temperature, T_5, $^\circ R$	1900	2000	2000, 2300 2600
Reactor fuel plate surface temperature, T_S, $^\circ R$	2060	2660 2960	2960
Fuel plate thickness, ϵ, in.	0.01	0.07 .01	0.01 .07

Case I, metal system. - The conditions of case I are representative of a system employing metal fuel elements. By the procedures indicated in the section "Methods" and in figure 8, a series of reactor diameters, reactor lengths, reactor heat releases, and aircraft gross weights were obtained and are indicated in figure 9. Figure 9 shows that for the operating conditions of case I the minimum reactor diameter is about 9.5 feet for a length of 3.25 feet. The corresponding reactor heat release is 520,000 Btu per second, exclusive of heat generated in the moderator; and the aircraft gross weight is 535,000 pounds. Figure 9 therefore indicates an incentive to achieve higher fuel element temperatures, in order to achieve small reactor diameters, reactor heat releases, and airplane gross weights. The results of the studies of cases II and III, which are representative of systems employing refractory materials, are accordingly discussed in detail as follows.

Case II - Performance with Ceramic Fuel Elements at Essentially Feasible Operating Conditions

Figures 10 to 12 represent data calculated for operating conditions regarded as feasible without much development of existing components.

A plot of the type shown in figure 8 provides accurate intersection points for defining the operating conditions for flight. An alternate plot, which gives the same intersection data but permits a more general insight into the nature of the system is shown in figure 10, which presents F_n/w_a as a function of w_a/A_R. The solid curve of figure 10 represents $(F_n)_{avail}/w_a$; and inasmuch as $(F_n)_{avail}/w_a$ depends only upon the temperature and pressure level and is independent of the external configuration, a unique curve is obtained regardless of d_R. The broken horizontal line represents the F_n/w_a that would be available if there were no pressure drop in the internal flow system (33 lb-sec/lb). The solid curve, representing the available F_n/w_a, is concave downward with a curvature that increases, because of increasing pressure drop, as w_a increases toward the choking value (choking value is not shown in the fig.). The dashed curves represent the $(F_n)_{req}/w_a$, obtained from equation (B12), for a series of d_R values. Figure 8 showed that the $(F_n)_{req}$ curve is nearly linear with w_a; consequently, $(F_n)_{req}/w_a$ shown in figure 10 is nearly hyperbolic with w_a and levels off as w_a increases. It may be seen, therefore, from figure 10, that d_R values much smaller than 8 feet are not feasible.

Relation between reactor diameter and performance parameters. - Figure 11(a) is a plot of the minimum feasible w_a/A_R against the values of d_R obtained by intersection of the required and available F_n curves of figure 10; and figures 11(b) to 11(h) show the corresponding values of l_R, P_5/P_2, F_n/w_a, W_{sh}, w_a, total engine weight, and total engine thrust. As d_R decreases from 10 to 8 feet, w_a/A_R increases from 35 to 60 pounds per second per square foot (fig. 11(a)); l_R increases from 2.92 to 3.25 feet (fig. 11(b)); P_5/P_2 decreases from 0.885 to 0.655 (fig. 11(c)), (the component pressure ratios entering into P_5/P_2 are also shown in fig. 11(c)); F_n/w_a decreases from 31.6 to 26.3 (fig. 11(d)); W_{sh} decreases from 205,000 to 180,000 pounds (fig. 11(e)); w_a decreases slightly from 2750 pounds per second and then increases to 3000 pounds per second (fig. 11(f)); the engine weight follows the air flow variation and ranges from 76,000 to 87,000 pounds (fig. 11(g)); the F_n decreases steadily from 87,000 to 79,000 pounds (fig. 11(h)) because F_n/w_a decreases more rapidly than w_a increases.

The opposing influences of decreasing W_{sh} and increasing engine weight are reflected in W_g shown in figure 12, which also shows the corresponding Q and airplane L/D. The value of W_g decreases to a minimum of about 480,000 pounds as d_R decreases to $8\frac{3}{4}$ feet and then increases as d_R decreases further. In spite of the increase in W_g and decrease in F_n, flight remains possible with d_R between $8\frac{3}{4}$ and 8 feet because the airplane L/D increases from 5.86 to 6.16 in this range of d_R. For d_R smaller than 8 feet, however, the increase in L/D is not enough to compensate for the rising engine weight and falling F_n; hence, flight ceases to be possible. The reactor power output in the range of operable d_R follows the variation in w_a, and is seen to have a minimum of about 494,000 Btu per second at a $9\frac{1}{4}$-foot d_R; thus, for the assumed operating conditions, Q is essentially 1 Btu per second per pound of W_g. (This power output neglects losses to the moderator.)

In order to present a more detailed picture of the foregoing results, a specific d_R was selected from a study of figures 10 to 12, and case IIA of table I was prepared. The 8.5-foot d_R indicated in case IIA of table I was selected by a compromise between the requirement of low W_g, near minimum d_R, and relative insensitivity of the performance parameters to d_R.

Gains from currently feasible ceramic fuel elements (case IIA). - It may be seen from a comparison of cases I and IIA (figs. 9 and 12) that if a ceramic fuel element is used, instead of the metal element of case I, the higher permissible T_S (2660° R) permits an increase in T_5 from 1900° R to 2000° R, which is approximately the temperature limit for uncooled turbines. The gains from the higher T_S and T_5 are a reduction of 1 foot in d_R, a reduction of about 40,000 pounds in W_g, and a reduction of about 25,000 Btu per second in Q. These gains are achieved in spite of the 0.07-inch ceramic fuel plate thickness, as compared with the 0.01-inch metal plate thickness.

Effect of ceramic fuel plate thickness. - It is of interest to determine whether a large reduction in ceramic plate thickness produces significant further gains over the performance of case IIA if P_2/P_1, T_S, and T_5 are left unchanged. Accordingly, computations were made for a ceramic plate thickness of 0.01 inch, herein designated as case IIB, and the comparison of cases IIA and IIB is shown in figure 13.

The analysis for case IIB showed that with the 0.01-inch ceramic plate the minimum suitable d_R is about 8 feet. Figure 13 shows that for the 8-foot d_R the corresponding W_g is 442,000 pounds, Q is 450,000 Btu per second, and l_R is 3.28 feet. Thus, for approximately the same l_R in cases IIA and IIB, the reduction in ϵ from 0.07 to 0.01 inch results in a decrease of about half a foot in d_R and 38,000 pounds in W_g. (Substantial gains from thin plates are indicated when the thermal stresses are considered in the following section.) A more detailed picture of case IIB is shown in table I.

Thermal stress. - The experimentally determined (ref. 10) thermal conductivity K of molybdenum disilicide $MoSi_2$ in the temperature range 700° to 1460° R is shown by the solid line in figure 14(a). In the indicated temperature range, K is linear with temperature and decreases substantially as temperature increases. The indicated substantial decrease in K suggested that K might be quite low at the high T_S herein investigated, and might be decreasing further in the plate interior. When K was extrapolated to temperatures of about 3000° R, several variations were considered; dotted lines joining the K value at 1460° R to several possible values at 2960° R are shown in the figure.

The steady-state thermal stress at the surface of a heat-generating plate of linearly varying conductivity is shown in figure 14(b). The figure is from reference 9 and presents the dimensionless surface stress

$\sigma_S(1-\nu)/\beta E\theta_S$ over a range of values of $q'''\epsilon^2/8K_{pe}\theta$ for several possible values of the ratio K_{pS}/K_{pe}. By use of this figure, and on the basis of the method discussed in reference 9 and appendix D, steady-state thermal stresses for several possible conductivity variations were computed for the reactor presented in case I of table I of this report. These computed values are rounded to three figures in the following table.

STEADY-STATE STRESS AT PLATE SURFACE NEAR REACTOR INLET

Reactor identity	Plate thickness, ϵ, in.	h_{av}, $\frac{\text{Btu}}{\text{sec ft}^2\ ^\circ\text{R}}$	$q'''\epsilon^2/8K_{pe}\theta_S \cong \frac{1}{4}\frac{h_{av}\epsilon}{K_{pe}}$	$\frac{K_{pS}}{K_{pe}}$	$\frac{\sigma_S(1-\nu)}{\beta E\theta_S}$	σ_S, psi
Case IIA	0.07	0.0723	0.01583	0.312	0.03787	21,600
				.500	.02177	12,400
				1.00	.01056	6,020
Case IIB	0.01	0.0600	0.001877	0.312	0.004066	2,320
				.500	.002512	1,430
				1.00	.001252	715

2659

The table shows that if the properties of fuel-impregnated $MoSi_2$ are the same as those of pure $MoSi_2$, and if the slope of the conductivity line of pure $MoSi_2$ remains constant throughout the range 700° to 2960° R (K_{ps}/K_{pe} = 0.312), the steady stress at the surface of the 0.07-inch plate, if elastic, would be 21,600 pounds per square inch. If the conductivity variation flattens out with temperature, the elastic stress would be lower. The table, together with figure 14(b), shows that except at very low values of K_{pS}/K_{pe} the reduction in stress is almost directly proportional to the improvement in conductivity and, for constant heat-transfer coefficient and air temperature, is also almost proportional to the decrease in plate thickness. Thus it is seen that a substantial reduction in stress occurs from reduction of plate thickness or improvement in thermal conductivity. (Further investigation is required to determine whether the actual magnitudes of the tabulated stresses are valid, because at the 2660° R surface temperature postulated for case II the thermal stress might be largely relieved by creep of the material. Basically the tabulated stresses indicate the desirability of determining experimentally the thermal conductivity and creep properties of fuel-impregnated $MoSi_2$ at the elevated temperatures herein postulated for the reactor calculations. For other high-temperature materials of the same thickness and temperature, the stresses would generally be different from those computed for $MoSi_2$, while the reactor dimensions for a prescribed reactor heat release would be the same.)

Thermal shock. - The question of the thermal shock that might occur on emergency shut-down of the reactor is of interest to consider. The precise evaluation of the shock requires a knowledge of the air flow and temperature existing in the reactor in the first fractions of a second following reactor shut-down. In the absence of such information, a reasonable first approximation is to assume that both the air flow and the air temperature are the same as in the steady state. It is shown in reference 9 that if the cooling conditions at the surface are the same in the steady and initial transient states, the maximum stresses are equal in the steady and in the transient states; hence, as a first approximation the thermal shock is no more serious than the steady-state thermal stress. Reactor after-heat would tend, also, to alleviate thermal shock.

Remarks on cases I and II. - It is of interest that if the thermal stress can be shown experimentally to be tolerable, then flight with the direct-air cycle at 35,000 feet at $M = 1.5$ is theoretically possible with engine and reactor components that may be feasible without much development work (cases I and IIA).

It is noteworthy that the operating conditions of cases I and II favor W_g at the expense of fuel investment. For example, the assumption of an isothermal reactor wall, which leads to shorter reactors, implies a relatively high fuel investment. Further, the reactor diameter-to-length ratio d_R/l_R of about 3, obtained for cases I and II, is also not optimum from a fuel investment viewpoint. Changes in d_R/l_R obtained by changes in l_R lead to undesirable results. (It may be shown that l_R values greater than 3 feet, obtained by increases in α, lead to an undesirable increase in W_g. Reactor lengths shorter than 3 feet, with resulting slight reductions in d_R and W_g, are possible by reducing α; but the resulting d_R/l_R increases, and the fuel investment would also increase.) Hence, better values of d_R/l_R must be obtained by decreases in d_R. If T_S, T_5, and P_2/P_1 are limited to 2660° R, 2000° R, and 15, respectively, remaining factors that might lead to smaller d_R by reducing pressure drop for a given air flow are shield free flow ratio and shield tube diameter, which were not optimized in this analysis. The assumed free flow ratios of 0.3 and about 0.4 in the upstream and downstream shields, respectively, for the indicated operating conditions may be unnecessarily conservative. The upstream shield pressure drop would decrease by 40 or 60 percent if the free flow ratio increased to 0.4 or 0.5; the downstream shield pressure drop would decrease by 35 percent if the free flow ratio increased to 0.5. (For a fixed number of shield-tube bends, an increase in the shield free flow ratio implies an increased alinement of alternate straight portions of the tube.) The shield pressure drop would

also decrease if the number of 30° bends were reduced from four to two. A determination of the largest shield free flow ratio and minimum number of bends compatible with neutron shielding for a shield construction as shown in figures 2 and 3 would be desirable. Shield pressure drop might also be reduced by increasing the shield-tube diamter, which for the indicated operating conditions was about 1 inch at w_a/A_R area of about 50 pounds per second per square foot.

Case III - performance at more optimistic operating conditions. - As T_S increases and ϵ decreases, the required α to yield a prescribed l_R may be expected to increase. The resulting decrease in reactor pressure drop and improvement in the remaining cycle performance parameters make possible a decrease in l_R. Furthermore, it was evident from figures 10 to 13 that if the level of $(F_n)_{avail}$ were increased by increasing the operating temperature, and if the pressure drop were decreased, the minimum operable reactor diameter could be decreased. Consequently, a preliminary evaluation has been made of the incentive to develop reactor and turbine materials of higher operating temperatures, fuel plates of lower thickness, and compressors of higher pressure ratios than those currently available. For this phase of the study, a T_S of 2960° R and ϵ of 0.01 inch were assumed, and T_5 of 2000°, 2300°, and 2600° R and P_2/P_1 of 15, 20, and 25 were explored. In addition, α was examined in considerable detail for determination of suitable values.

Selection of reactor free flow ratio. - The reactor design calculations indicated that l_R was extremely sensitive to α. In order to determine whether the over-all aircraft performance was equally sensitive to α, W_g and Q were determined as functions of l_R at the following operating conditions: T_S = 2960° R; P_2/P_1 = 15; T_S = 2600° R; α = 0.49 and 0.50. The results of these calculations are shown in figure 15. It is seen that for α of 0.50, l_R is approximately 6 feet, and substantial decreases appear desirable. A decrease in α to 0.49 results in a decrease of about 3 feet in l_R, and in a decrease of about 50,000 pounds in W_g. Thus if substantial decreases in l_R are possible, W_g is sensitive to α. (If l_R is already in the neighborhood of 3 ft, however, substantial decreases in l_R are not desirable from a fuel-investment viewpoint.)

In cases I and II, d_R values of approximately 9 feet were obtained when l_R was about 3 feet, chosen to favor W_g at the probable expense of fuel investment. Inasmuch as the use of higher T_S, higher T_5, and smaller ϵ favors smaller d_R (about 5 ft, fig. 15), l_R between 2 and

4 feet appeared to be suitable for case III from the viewpoints of fuel investment and control, as well as W_g. The values of α were chosen from the data presented in figures 16 and 17, which show l_R as a function of w_a/A_R at various α values. Figure 16 presents data for a constant P_2/P_1 of 15 and T_5 of 2000°, 2300°, and 2600° R; figure 17 presents data for a constant T_5 of 2600° R and P_2/P_1 of 15, 20, and 25. From figure 16, α was selected to be 0.5 for T_5 of 2000° and 2300° R, and an α of 0.49 was selected for a T_5 of 2600° R. From figure 17 an α value of 0.5 was selected for all three values of P_2/P_1 (15, 20, and 25).

Effect of turbine-inlet temperature. - Figure 17 is analogous to figure 10 of case II and shows the curves of available and required F_n as functions of w_a/A_R for T_5 of 2000°, 2300°, and 2600° R, at a P_2/P_1 of 15, and for d_R of 5, 7, and 10 feet. The value of α at each T_5 is also indicated on the figure. The solid curves, representing $(F_n)_{avail}$, are uniquely determined by the temperatures and pressures of the system. The dashed curves in the figure represent within ±3 percent the $(F_n)_{req}$ at the indicated d_R and T_5. ($(F_n)_{req}$ at any d_R varies slightly with T_5; for clarity in fig. 16, curves of average $(F_n)_{req}$ are presented.) Figure 18 shows that as T_5 increases from 2000° to 2600° R, the maximum available F_n/w_a increases from about 30 to about 60 pound-seconds per pound, and the minimum operable d_R decreases from about 7 to about 4 feet.

Figure 19 shows the values of performance parameters as functions of d_R for the same operating conditions as listed for figure 18. In figure 19(a) are shown w_a, total engine weight, l_R, and W_{sh}. This figure shows that at each value of T_5, w_a decreases steadily to a minimum as the operable d_R decreases, and the total engine weight follows the variation in w_a. The figure also shows that although l_R increases, W_{sh} steadily decreases, as operable d_R decreases from large to minimum values at each value of T_5.

As T_5 increases from 2000° to 2600° R, w_a at the minimum d_R decreases, reflecting the increase in available F_n/w_a discussed under figure 18. The value of l_R, which would increase steadily with temperature if α were constant, shows no consistent variation with temperature in figure 19(a) because α was varied as previously discussed. The variation in W_{sh} with temperature at a fixed d_R reflects the variation in l_R.

In figure 19(b) are shown W_g, Q (exclusive of heat lost to the moderator), and airplane L/D. As T_5 increases from 2000° to 2600° R, the minimum W_g decreases from 410,000 to 291,000 pounds at minimum operable d_R of $7\frac{1}{2}$ and 5 feet, respectively; the minimum Q decreases from 425,000 to 332,000 Btu per second; and the airplane L/D decreases from 5.84 to 5.52.

In order to show a more detailed picture of the foregoing results, as in case II, a specific d_R (5.0 ft) was selected from a study of figures 18 and 19, and case IIIA of table I was prepared. Results for a T_5 of 2600° R, at α of 0.49, are shown in the table. As in case II, the d_R indicated in the table was selected by a compromise between the requirements of low W_g and relative insensitivity of the performance parameters to d_R.

Effect of fuel plate thickness. - Inasmuch as the high T_S and T_5 and small ϵ of case III result in attractive values of d_R and W_g, it is of interest to determine whether the performance is significantly impaired by the use of thicker fuel plates. Accordingly, computations were made for ϵ of 0.07 inch herein designated as case IIIB, and a comparison of cases IIIA and IIIB is shown in figure 20.

The analysis for case IIIB showed that with the 0.07-inch ceramic plates, the minimum suitable d_R is about 5.5 feet; the corresponding W_g is 318,000 pounds, Q is about 370,000 Btu per second; and l_R is 4.1 feet. Thus, for the same l_R in cases IIIA and IIIB, the increase in ϵ from 0.01 to 0.07 inch results in an increase of 0.5 foot in d_R and 27,000 pounds in W_g. The relative stresses for the two values of ϵ are discussed later. A more detailed picture of case IIIB is shown in table I.

Effect of compressor pressure ratio. - Figure 21, which is analogous to figure 10 of case IIA and figure 18 of case IIIA, shows the curves of available and required F_n/w_a as functions of w_a/A_R for P_2/P_1 of 15, 20, and 25, at T_5 of 2600° R, and for d_R of 4, 5, 7, and 10 feet. The value of α for all cases was 0.49. The solid curves, representing $(F_n)_{avail}$, are uniquely determined by the temperature and pressures of the systems. The dashed curves of the figure represent within ± 1 percent the $(F_n)_{req}$ at the indicated d_R and P_2/P_1. The figure shows that although the minimum attainable d_R is slightly less than 4 feet for a P_2/P_1 of 25, a d_R of 4 feet is possible at P_2/P_1

of 20, and d_R values smaller than 5 feet are possible for a P_2/P_1 of 15; hence, a P_2/P_1 between 15 and 20 appears the best practical choice for T_5 of 2600° R.

Figure 22 shows the values of performance parameters as functions of d_R for the same operating conditions as listed for figure 21. In figure 22(a) are shown w_a, total engine weight, l_R, and W_{sh}; in figure 22(b) are shown W_g, Q exclusive of losses, and airplane L/D. Figure 22 shows that at each value of P_2/P_1 the variations of the parameters with d_R are essentially the same as those shown in figure 19. Examination of figure 22 indicates only slight variation of the over-all parameters with P_2/P_1. Although the figures show that a P_2/P_1 value of 25 gives the lowest d_R, W_g, and Q, the curves also indicate that the performances at the lower P_2/P_1 are only slightly inferior, and hence that a P_2/P_1 between 15 and 20 appears a suitable choice for T_5 of 2600° R. The detailed performance at a P_2/P_1 of 15 has been discussed and a suitable point is tabulated as case IIIA of table I. A similar tabulation for the best point of the analysis (P_2/P_1, 25), herein designated as case IIIC, is also presented in table I.

Thermal stresses. - The steady-state fuel-surface stresses for the reactors designated as case IIIA, IIIB, and IIIC of table I of this report were computed to be as follows:

Reactor designation, Case III	Plate thickness, ε, in.	h_{av}, $\frac{\text{Btu}}{\text{sec ft}^2\ ^\circ\text{F}}$	$\frac{q'''\varepsilon^2}{8K_{pe}\theta_S}$	$\frac{K_{pS}}{K_{pe}}$	$\frac{\sigma_S(1-\nu)}{\beta E\theta_S}$	σ_S, psi
A	0.01	0.069	0.002158	0.151	0.010296	7,200
				.500	.002889	2,020
				1.000	.001439	1,010
B	0.07	0.083	0.01817	0.151	--------	------
				.500	0.02510	17,600
				1.000	.01212	8,480
C	0.01	0.103	0.003637	0.170	0.01577	9,500
				.500	.00488	2,940
				1.000	.00243	1,460

The stress table shows, as previously under case II, that the stress is strongly dependent on plate thickness and conductivity.

It is noteworthy for the 0.07-inch plate of case IIIB that the heat generation parameter $q'''\varepsilon^2/8K_{pe}\theta_S$ has too large a value if the conductivity of $MoSi_2$ continues to decrease at the rate shown in figure 14(a) in the temperature range between 700° and 1460° R. For the combination $q'''\varepsilon^2/8K_{pe}\theta_S = 0.01817$ and $K_{pS}/K_{pe} = 0.151$, the conductivity in the plate interior becomes "zero," as indicated in reference 9. The thermal stress for this case cannot be computed. Even for K_{pS}/K_{pe} equal to 0.50, the stress exceeds 17,000 pounds per square inch and the desirability of plates thinner than 0.07 inch is evident. Concerning thermal shock, it may be assumed, as indicated in case II, that the maximum transient stress will not differ substantially from the steady-state value.

Summary comparison of cases I, II, and III. - For ready comparison of the principal cases herein considered, figure 23 is presented. The individual curves of the figure have already been discussed in detail in the body of the report.

SUMMARY OF RESULTS

A study has been made of some considerations involved in the use of high-temperature materials for a nuclear-powered direct-air-cycle aircraft to fly at 35,000 feet at a Mach number of 1.5. For the assumptions made herein the results are as follows:

1. For a system employing metal elements of 0.01-inch thickness and operating at a compressor pressure ratio of 15, a reactor fuel temperature of 2060° R, and a turbine-inlet temperature of 1900° R, the smallest reactor diameter was about 9.5 feet, and the aircraft gross weight was about 535,000 pounds.

2. For design conditions that may not require much development, namely a system employing ceramic elements of 0.07-inch thickness, and operating at a compressor pressure ratio of 15, a reactor fuel temperature of 2660° R, and turbine-inlet temperature of 2000° R, the smallest reactor diameter was about 8.5 feet, and the aircraft gross weight was about 480,000 pounds. When the plate thickness was reduced to 0.01 inch and all other conditions were left unchanged, the smallest reactor diameter was 8.0 feet and the gross weight 442,000 pounds. The thermal stresses in the 0.01-inch plate were less than one-seventh of the stresses in the 0.07-inch plate.

3. For temperatures in the range that requires major materials development (reactor plate surface temperature, 2960° R; turbine-inlet temperatures greater than 2000° R) the gross weight and the reactor diameter both decreased with increasing turbine-inlet temperature in the range investigated (2000°, 2300°, 2600° R).

4. For a ceramic system employing fuel elements of 0.01-inch thickness and operating at a compressor pressure ratio of 15, a reactor fuel temperature of 2960° R, and a turbine-inlet temperature of 2600° R, the smallest reactor diameter was about 5.0 feet, and the aircraft gross weight was about 292,000 pounds. When the plate thickness was increased to 0.07 inch and all other conditions were left unchanged, the smallest reactor diameter was 5.5 feet and the gross weight about 318,000 pounds. The thermal stresses in the 0.01-inch plate were less than one-eighth of the stresses in the 0.07-inch plate.

5. For compressor pressure ratios in the range requiring component development (pressure ratios greater than 15) the gross weight and reactor diameter decreased only slightly with increasing pressure ratio in the range investigated (15, 20, and 25).

6. The most attractive performance on the basis of reactor diameter, reactor heat release, and airplane gross weight was obtained for a reactor fuel plate surface temperature of 2960° R, a turbine-inlet temperature of 2600° R, and a compressor pressure ratio of 25. For these conditions and for a fuel plate thickness of 0.01 inch the performance was as follows: reactor diameter, 4 feet; reactor length, 4.0 feet; airplane gross weight, 279,000 pounds; and reactor heat release, 284,000 Btu per second. This performance was only slightly better than the best performance at a compressor pressure ratio of 15.

Lewis Flight Propulsion Laboratory
National Advisory Committee for Aeronautics
Cleveland, Ohio, November 17, 1952

APPENDIX A

SYMBOLS

The following symbols are used in this report:

A_a	air flow area, sq ft
A_c	compressor frontal area, sq ft
A_d	area downstream of sudden expansion or contraction, sq ft
A_F	fuselage frontal area, sq ft
A_0	full expansion nozzle exit area, sq ft
A_R	reactor frontal area, sq ft
A_u	area upstream of sudden expansion or contraction, sq ft
C_D	coefficient of wave drag
C_f	coefficient of friction
C_L	lift coefficient
$(C_L)_{max}$	maximum lift coefficient at landing
$(C_L)_{opt}$	optimum lift coefficient at design condition
C_v	exhaust nozzle velocity coefficient
c_p	specific heat at constant pressure, Btu/lb-^oR
$c_{p,\phi}$	specific heat evaluated at average film temperature, Btu/lb-^oR
c_v	specific heat at constant volume, Btu/lb-^oR
D_F	fuselage drag, lb
D_f	friction drag, lb
D_N	boattail drag, lb
D_{nose}	nose section drag, lb

D_t	tail drag, lb
D_W	wave drag, lb
D_w	wing drag, lb
D_y	main body section drag, lb
D_z	boattail section drag, lb
d_c	compressor diameter, ft
d_e	equivalent diameter, ft
d_F	fuselage diameter, ft
d_F'	engine circle diameter, ft
d_h	turbine hub diameter, ft
d_O	nozzle exit diameter, ft
d_R	reactor diameter, ft
d_x	nose cone base diameter, ft
E	modulus of elasticity, lb/sq in.
F_j	jet thrust, lb
F_n	net thrust, lb
$(F_n)_{avail}$	available net thrust, lb
$(F_n)_{req}$	required net thrust, lb
f	friction factor
f_ϕ	friction factor based on modified film Reynolds number
G	mass velocity, ρV, lb/sq ft-sec
g	acceleration due to gravity, ft/(sec)^2
h	local heat transfer coefficient, Btu/sec-sq ft-$^\circ$R
h_{av}	average heat transfer coefficient in reactor, Btu/sec-sq ft-$^\circ$R

J	mechanical equivalent of heat, ft-lb/Btu
K	thermal conductivity, Btu/sec-ft-^{o}R
K_{pe}	conductivity of plate material at temperature of cooling environment, Btu/sec-ft-^{o}R
K_{pS}	conductivity of plate material at temperature of plate surface, Btu/sec-ft-^{o}R
K_{ϕ}	conductivity of air at average film temperature, Btu/sec-ft-^{o}R
L/D	airplane lift-drag ratio
$(L/D)_{max}$	maximum possible wing lift-drag ratio at design conditions
$(L/D)_{w}$	actual wing lift-drag ratio
l	length, ft
l_{b}	diffuser length, ft
l_{c}	compressor length, ft
l_{N}	slant height of boattail section, ft
l_{p}	plenum chamber length, ft
l_{R}	reactor length, ft
l_{T}	turbine length, ft
l_{x}	length of nose cone section, ft
$l_{x,1}$	length of nose cylindrical section, ft
l_{y}	length of main body section, ft
$l_{y,1}$	distance from diffuser inlet to face of end shield, ft
l_{z}	length of boattail section, ft
M	Mach number
M_{u}	Mach number upstream of sudden expansion or contraction
P	total pressure, lb/sq ft

p	static pressure, lb/sq ft
p_d	static pressure downstream of sudden expansion or contraction, lb/sq ft
p_u	static pressure upstream of sudden expansion or contraction, lb/sq ft
Pr_ϕ	Prandtl number with gas properties evaluated at average film temperature
Q	reactor heat release rate, Btu/sec
q	dynamic pressure, lb/sq ft
q''	heat flow rate per unit area, Btu/sec-sq ft
q'''	volumetric heat generation rate, Btu/sec-cu ft
R	gas constant for air, 53.4 ft-lb/lb-$^\circ$R
Re_ϕ	modified Reynolds number with gas properties evaluated at average film temperature
S_R	reactor heat-transfer surface, sq ft
S_w	surface area of wing, sq ft
T_a	air total temperature, $^\circ$R
T_{av}	average total temperature, $^\circ$R
T_e	total temperature of cooling environment, $^\circ$R
T_S or t_S	reactor fuel plate surface temperature, $^\circ$R
T_ϕ	film total temperature, $^\circ$R
t	static temperature, $^\circ$R
t_{av}	average static temperature, $^\circ$R
t_ϕ	film static temperature, $^\circ$R
V	velocity, ft/sec
V_d	velocity downstream of sudden expansion or contraction, ft/sec

V_l	landing speed, ft/sec
V_u	velocity upstream of sudden expansion or contraction, ft/sec
V_R	volume of reactor fuel plate, cu ft
W_c	compressor weight, lb
W_g	airplane gross weight, lb
W_R	reactor weight, lb
W_s	structure weight, lb
W_{sh}	shield weight, lb
W_T	turbine weight, lb
w_a	air flow, lb/sec
α	reactor free flow ratio
β	coefficient of thermal expansion, ft/ft-$^\circ$R
γ	ratio of specific heats, c_p/c_v
δ	ratio of total pressure at flight condition to sea level static pressure, P/2116
Δp	static pressure drop, lb/sq ft
Δp_f	friction pressure drop, lb/sq ft
Δp_m	momentum pressure drop, lb/sq ft
ϵ	reactor fuel plate thickness, in. or ft
θ	ratio of total temperature at flight condition to sea level static temperature, T/519
θ_s	temperature difference between fuel plate surface and cooling environment, $^\circ$R
μ_ϕ	air viscosity at average film temperature, lb/sec-ft
ν	Poisson's ratio

2659

ρ	weight density, lb/cu ft
ρ_{av}	average air density, lb/cu ft
$\rho_{av,R}$	average reactor density, lb/cu ft
ρ_d	density downstream of sudden expansion or contraction, lb/cu ft
ρ_{sl}	sea level standard density, lb/cu ft
ρ_u	density upstream of sudden expansion or contraction, lb/cu ft
σ_S	stress at surface of reactor fuel plate, lb/sq in.
σ_{SO}^*	dimensionless steady-state surface stress

Subscripts:

0	free stream
1	compressor inlet
2	compressor outlet
3	reactor inlet
4	reactor outlet
5	turbine inlet
6	turbine outlet

APPENDIX B

AIRPLANE CONFIGURATION AND METHODS OF PERFORMANCE CALCULATION

This appendix presents the procedure employed in the report in determining the airplane design-point configuration, aerodynamic drag of wing-body configuration, component sizes and weights, and the engine cycle performance.

Configuration

Selection of wing. - A delta wing was assumed having a double-wedge airfoil section, 4 percent thick, with a maximum thickness at 20 percent chord. The sweep angle and the data for calculating the wing L/D were taken from an unpublished NACA survey for supersonic aircraft. The method of determining the wing L/D is presented later.

Fuselage. - Design of the fuselage (fig. 1) consisted in: (1) Determining the length and diameter of the main body section required to house the diffuser, engines, reactor, and shield; (2) dimensioning the nose section to provide space for the crew compartment, a 50-foot separation between the crew compartment and reactor shield face, and good aerodynamic characteristics (low over-all drag) for this section; and (3) determining the boattail length and taper angle to provide an adequate full-expansion exhaust nozzle with minimum drag.

Main body section. - The diameter of the main section was determined by the larger of the quantities: engine circle diameter d_F' or the shield support outside diameter d_F as shown in figure 5. The value of d_F' was obtained by assuming six engines located in a ring (fig. 5) with w_a/A_c of 30 pounds per second per square foot. This flow corresponds to a compressor-inlet Mach number of 0.65. Thus,

$$\frac{w_a}{A_c}\frac{\sqrt{\theta_1}}{\delta_1} = 30 \text{ lb/sq ft} \tag{B1}$$

and for each engine

$$A_c = \frac{1}{6}\ \frac{1}{30}\ \frac{\sqrt{\theta_1}}{\delta_1}\ w_a \tag{B2}$$

The value of d_F (fig. 5(b)) was taken as d_R plus twice the sum of 5-inch reflector thickness, the 36-inch shield thickness, and the 6-inch support ring thickness.

The length of the fuselage main section was determined by the lengths of the internal components (that is, diffuser, compressor, two plenum chambers, reactor, shield, and turbine, see fig. 5). A design-point diffuser was assumed, and the air inlet was visualized as an annular space surrounding the base of the nose cone. Assumptions for component lengths were as follows: (1) diffuser length l_b, 6 feet; (2) the compressor length l_c, 1.5 times its diameter which was determined from equation (B2); (3) the plenum chamber lengths l_p, 1.0 foot each, which allows sufficient area in a radial direction for the air to enter and leave the shield; (4) 6 feet of water for the sum of the end-shield thicknesses; (5) turbine length, l_T 2 feet; and (6) a shadow shield and miscellaneous requirements, 6 inches. (l_R was determined from the heat-transfer calculations.) The sum of these lengths composes the length of the main body section, l_y:

$$l_y = 1.5\ d_c + l_R + 16.5 \tag{B3}$$

$$l_{y,1} = 1.5\ d_c + l_b = 1.5\ d_c + 6 \tag{B4}$$

Nose section. - The nose section was assumed to be a cone plus a cylinder (fig. 6). The cone base-to-height ratio $(l/d)_x$ is 6, (vertex angle of 9.6°), corresponding to approximate minimum friction plus wave drag. The length of the cylindrical section was in every case adjusted to maintain the crew compartment at a distance of 50 feet from the shield face. The nose cone base diameter d_x was determined by the required flow area at the diffuser inlet and the previously determined fuselage main section diameter d_F (fig. 6).

$$\frac{\pi}{4}\ d_x^2 = \frac{\pi}{4}\ d_F^2 - A_a \tag{B5}$$

where for a flight Mach number of 1.5,

$$\frac{w_a\sqrt{\theta_1}}{A_a\delta_1} = 42.75 \quad \text{or} \quad A_a = \frac{w_a}{32.75} \tag{B6}$$

therefore from equations (B5) and (B6)

$$d_x = \sqrt{d_F^2 - \frac{w_a}{25.7}} \tag{B7}$$

For the range of air flows considered, the corresponding cone height $l_x = 6d_x$ is always greater than 60 feet and will accommodate the crew compartment, the dimensions of which were taken from reference 1. In figure 6 it is seen that a fixed length of 60 feet was assumed from the rear of the crew compartment to the cone vertex. As the air flow is increased for a fixed d_F, d_x becomes smaller in order to provide passage for the air, and l_x becomes shorter. Consequently the cylindrical section $l_{x,1}$ must become longer in order to maintain the 50-foot separation between crew compartment and shield face. Thus, in the analysis the distance from the cone apex to the shield face is fixed at 110 feet. The lengths l_x, $l_{x,1}$, and l_y vary with air flow and fuselage diameter.

$$l_{x,1} = 110 - (l_x + l_{y,1}) \tag{B8}$$

where

$$l_x = 6d_x$$

and from equation (B4)

$$l_{y,1} = 1.5\ d_c + 6.0$$

Boattail section. - The exhaust gases from the six turbines were assumed to discharge into a single exhaust area (fig. 7). The area ratio A_0/A_F was determined, and the ratio of nozzle length to base diameter l_z/d_F was optimized using wave drag coefficients from reference 11 to give minimum boattail wave plus friction drag. Assumptions for the calculations were:

(1) turbine-exit Mach number $M_6 = 0.70$

(2) turbine hub-tip ratio $d_h/d_T = 0.60$

(3) A_0/A_6 determined at P_6/p_0 for a full expansion nozzle.

The equation obtained for determining A_0/A_F and d_0 is:

$$\frac{A_0}{A_F} = \left(\frac{d_0}{d_F}\right)^2 = \left(\frac{1.88\ T_6}{P_6}\right)\left(\frac{w_a}{A_F}\right)\frac{A_0}{A_6} \tag{B9}$$

The nozzle surface length l_N in terms of d_0, d_F, and l_z is:

$$l_N = \sqrt{\left(\frac{d_F - d_0}{2}\right)^2 + l_z^2} \tag{B10}$$

Aerodynamic Drag

Wing and tail drag. - The required thrust for level flight is given by:

$$(F_n)_{req} = D_w + D_t + D_F \tag{B11}$$

The wing drag D_w is a function of the airplane gross weight and wing lift-drag ratio. The tail drag D_t was assumed to be 10 percent of the wing drag. Therefore, equation (B11) becomes

$$(F_n)_{req} = \frac{1.1\ W_g}{(L/D)_w} + D_F \tag{B12}$$

The wing lift-drag ratio was obtained from an unpublished NACA analysis on maximum wing L/D for supersonic flight, and containing data on optimum design lift coefficients and maximum wing L/D. The following equation was derived from standard lift-drag relations,

$$(L/D)_w = \frac{\frac{W_g}{S_w}\frac{1}{q_0}}{\frac{1}{2\left(\frac{L}{D}\right)_{max}}\left[(C_L)_{opt} + \frac{\left(\frac{W_g}{S_w}\right)^2 \frac{1}{q_0{}^2}}{(C_L)_{opt}}\right]} \tag{B13}$$

where the wing loading W_g/S_w is given by:

$$\frac{W_g}{S_w} = (C_L)_{max}\ \frac{\rho_{sl}}{2g} V_l{}^2 \tag{B14}$$

These equations were solved with the aid of the following assumptions:

(1) a 4 percent thick delta wing

(2) maximum wing thickness at 20 percent chord

(3) a landing speed V_l of 150 mph

(4) a maximum landing lift coefficient $(C_L)_{max,l}$ of 1.335 (ref. 12)

(5) optimum lift-coefficient at the design point $(C_L)_{opt}$ of 0.185

(6) the maximum possible wing lift-drag ratio $(L/D)_{max}$ at the flight Mach number of 1.5 is 10.1

(7) the wing skin friction drag coefficient used to obtain the $(L/D)_{max}$ is 0.006

From equation (14) and the assumptions

$$W_g/S_w = 76.8 \text{ lb/sq ft}$$

From equation (B13) and the assumptions listed, the operating wing L/D is:

$$(L/D)_w = 8.3$$

Fuselage drag. - The fuselage drag consists of the wave and friction drag of the nose, main, and boattail sections.

The nose section drag consists of the cone drag and straight section drag (fig. 6). The cone was assumed to have the von Kármán parabolic profile (ref. 13) and its wave drag is given by

$$D_{W,x} = A_x q_0 \frac{d_x^2}{l_x} \tag{B15}$$

The cone friction drag is given by:

$$D_{f,x} = \pi d_x C_{f,x} \frac{l_x}{\cos 4.8^\circ} q_0 \tag{B16}$$

From reference 14 an average Reynolds number of 280×10^6 was obtained for the cone, and from reference 11 a corresponding friction coefficient was obtained.

$$C_{f,x} = 0.002$$

The drag for the straight section of the nose $l_{x,1}$ is given by

$$D_{f,x,1} = \pi d_x \, l_{x,1} \, q_0 \, C_{f,x,1} \tag{B17}$$

where $C_{f,x,1} = 0.0025$ corresponding to a Reynolds number of 86×10^6.

Combining equations (B15), (B16), and (B17), and substituting the values of C_f, q_0, l_x used in this analysis result in

$$D_{nose} = 31.9\ d_x^2 + 6.15\ d_x\ (110 - l_{y,1} - 6d_x) \tag{B18}$$

The main section consists of a cylindrical surface and only friction drag was considered.

$$D_{f,y} = \pi d_F\ l_y\ q_0\ C_{f,y} \tag{B19}$$

where $C_{f,y} = 0.0023$, corresponding to an average Reynolds number of 75×10^6.

Thus,

$$D_{f,y} = 5.66 \times 0.0023\ (1.5\ d_c + l_R + 16.5) \tag{B20}$$

The boattail section consists of a truncated cone (fig. 7) and both friction and wave drag are considered.

$$D_{W,z} = C_D\ q_0\ A_F \tag{B21}$$

$$D_{f,z} = C_{f,z}\ q_0\ \pi \left(\frac{d_F + d_0}{2}\right) l_N \tag{B22}$$

For an average Reynolds number of 85×10^6, $C_{f,z} = 0.0025$. Combining equations (B21), (B22), and (B10) and $C_{f,z}$

$$D_N = q_0\ A_F \left[C_D + 0.005 \left(1 + \sqrt{\frac{A_0}{A_F}}\right) \sqrt{\frac{1}{4}\left(1 - \frac{d_0}{d_F}\right)^2 + \left(\frac{l_z}{d_F}\right)^2}\right] \tag{B23}$$

Values of C_D corresponding to A_0/A_F and l_z/d_F were obtained from reference 11.

Weight Calculations

The following weight analysis was made to include the weight of structure, reactor, shield, engines, and auxiliary equipment.

Structure. - The structure was assumed to consist of wing, tail, body, landing gear, and all ducts and valves. The variation of structure weight was accounted for by assuming a constant ratio of structure-to-gross weight.

$$\frac{W_s}{W_g} = 0.375$$

The weight data for determining this ratio were obtained from reference 15.

Reactor. - The reactor weight was assumed to be composed of structure, moderator, and fuel materials occupying 48 percent of the reactor volume.

Water moderator volume = $0.65\ (0.48\ v_R)$

Aluminum structure volume = $0.15\ (0.48\ v_R)$

Insulating SiO_2 volume = $0.20\ (0.48\ v_R)$

Fuel plate volume = $(0.52 - \alpha)(v_R)$

Void volume = αv_R

The average reactor density for these assumptions is

$$\rho_{av,R} = 47.5 + 381\ (0.52 - \alpha) \tag{B24}$$

and the reactor weight

$$W_R = \left(\frac{\pi d_R^2}{4}\ l_R\right) \rho_{av,R} \tag{B25}$$

Shield weight. - A divided shield system was assumed, and the overall computed weight included:

(1) A 3-foot water shield around the reactor

$$W_{sh,1} = 62.4\ \frac{\pi}{4}\ (l_R + 6)\left[(d_R + 6.833)^2 - (d_R + 0.833)^2\right] + 62.4\ \frac{\pi}{4}\ (6)\ (d_R + 0.833)^2 \tag{B26}$$

(2) A lead shadow shield assumed to be a 2.5-inch-thick disk with a 0.015-inch steel cladding. The diameter was taken equal to the engine circle diameter (fig. 5).

$$W_{sh,2} = 117\ (3d_c)^2 \tag{B27}$$

(3) A 5-inch thick reflector around the reactor composed of beryllium and steel, the combined density of which is assumed to be 222.5 pounds per cubic foot.

$$W_{sh,3} = 222.5 \frac{\pi}{4} l_R \left[(d_R + 0.833)^2 - d_R^2\right] \quad \text{(B28)}$$

(4) A steel shell container 1/8-inch thick, surrounding the water shield.

$$W_{sh,4} = 8 (d_R + 6.833)^2 + 16 l_R (d_R + 6.833) \quad \text{(B29)}$$

(5) A crew compartment from reference 1.

$$W_{sh,5} = 40{,}000 \text{ lbs}$$

Engine. - The engine weight was assumed to consist of the combined weights of the compressors, turbines, and shafts. The compressor weight from reference 16 is

$$W_c = 467 w_a \frac{\sqrt{T_1}}{P_1} \ln\left(\frac{P_2}{P_1}\right) \quad \text{(B30)}$$

The turbine weight also from reference 16 is:

$$W_T = 1315 w_a \frac{\sqrt{T_5}}{P_5} \ln\left(\frac{P_5}{P_6}\right) \quad \text{(B31)}$$

The six shafts were assumed to be hollow, each with torsional strength equal to that calculated for a solid shaft in the following equation from reference 17:

$$\text{diameter of solid shaft} = 65.5 \sqrt[3]{\frac{\text{transmitted horsepower}}{(\text{rpm}) \times (\text{allowable shear stress})}}$$

The horsepower was computed from the compressor work, the speed was assumed to be 6000 rpm, and the allowable shear stress (ref. 17) was assumed to be 4000 pounds per square inch. The ratio of hollow shaft diameter to solid shaft diameter was assumed to be 1.030. The ratio of the inner to outer diameters of the hollow shaft is 0.54, and the weight of the hollow shaft is 0.751 of the solid shaft (ref. 17).

Cycle Performance

The methods of computing the cycle performance are the same as in reference 16. The assumptions for this analysis are:

diffuser total pressure ratio $\frac{P_1}{P_0}$	0.95
compressor small-stage efficiency	0.88
turbine adiabatic efficiency	0.90
exhaust-nozzle velocity coefficient (full expansion) C_v	0.97

The available net thrust per pound of air per second was obtained from the following equation:

$$(F_n)_{avail} = w_a\left(\frac{F_J}{w_a} - \frac{V_0}{g}\right) \tag{B32}$$

$$\frac{F_J}{w_a} = C_v\sqrt{\frac{2Jc_pT_6}{g}\left[1 - \left(\frac{p_0}{P_6}\right)^{\frac{\gamma-1}{\gamma}}\right]} \tag{B33}$$

where

$$\frac{P_6}{p_0} = \left(\frac{P_1}{P_0}\right)\times\left(\frac{P_0}{p_0}\right)\times\left(\frac{P_2}{P_1}\right)\times\left(\frac{P_5}{P_2}\right)\times\left(\frac{P_6}{P_5}\right)$$

and P_3/P_2 was determined from the pressure drop calculations.

APPENDIX C

SUDDEN EXPANSION AND CONTRACTION

The relations between upstream and downstream gas conditions for sudden expansion and sudden contraction of the duct were derived as follows. If the subscripts u and d represent upstream and downstream, respectively, and the remaining symbols are as defined in appendix A, the general energy equation for an adiabatic flow in which elevation terms are negligible is

$$\frac{p_u}{\rho_u} + \frac{V_u^2}{2g} + Jc_v t_u = \frac{p_d}{\rho_d} + \frac{V_d^2}{2g} + Jc_v t_d \tag{C1}$$

An alternate form of equation (C1) is obtained by use of the following relations:

$$c_p - c_v = R/J;$$

$$c_p/c_v = \gamma;$$

$$t = \frac{1}{R}\frac{p}{\rho}$$

By use of these relations, equation (C1) can be written

$$\frac{\gamma}{\gamma-1}\frac{p_u}{\rho_u} + \frac{V_u^2}{2g} = \frac{\gamma}{\gamma-1}\frac{p_d}{\rho_d} + \frac{V_d^2}{2g} \tag{C2}$$

and can then be rearranged as

$$\frac{p_u}{\rho_u}\left[1 - \left(\frac{p_d}{p_u}\right)\left(\frac{\rho_u}{\rho_d}\right)\right] = \frac{\gamma-1}{2}\frac{V_u^2}{\gamma g}\left[\left(\frac{V_d}{V_u}\right)^2 - 1\right] \tag{C3}$$

The Mach number of a gas flow is

$$M = \frac{V}{\sqrt{\frac{\gamma g p}{\rho}}}$$

or

$$\frac{V^2}{\gamma g} = \frac{p}{\rho} M^2 \tag{C4}$$

By use of equations (C4) in (C3),

$$\left[1 - \left(\frac{p_d}{p_u}\right)\left(\frac{\rho_u}{\rho_d}\right)\right] = \frac{\gamma-1}{2} M_u^2 \left[\left(\frac{V_d}{V_u}\right)^2 - 1\right] \tag{C5}$$

The continuity equation for a steady one-dimensional flow is

$$\rho_u A_u V_u = \rho_d A_d V_d$$

or

$$\frac{V_d}{V_u} = \frac{\rho_u}{\rho_d} \frac{A_u}{A_d} \tag{C6}$$

By use of equations (C6) in (C5)

$$\left[1 - \left(\frac{p_d}{p_u}\right)\left(\frac{\rho_u}{\rho_d}\right)\right] = \frac{\gamma-1}{2} M_u^2 \left[\left(\frac{\rho_u}{\rho_d}\right)^2 \left(\frac{A_u}{A_d}\right)^2 - 1\right] \tag{C7}$$

This equation was employed both for sudden expansions and for sudden contractions.

Sudden Expansion: - Momentum Equation

For subsonic flows the static pressure on face CF (accompanying sketch) has been established experimentally to be p_u, the same as that

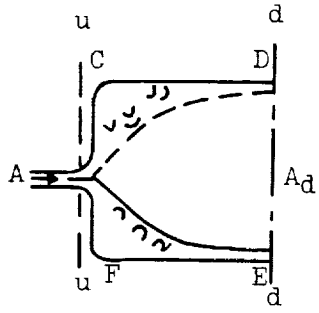

of the jet issuing from section u-u. The length CD in which the downstream pressure p_d is established is approximately 4.5 equivalent diameters of the upstream passage (ref. 8), and if the shear along the surface of the downstream passage in this short distance can be

neglected the net axial force on the fluid is $(p_u-p_d)A_d$. The rate of change of axial momentum is $\frac{w_a}{g}(V_d-V_u)$. Then

$$(p_u-p_d)A_d = \frac{w_a}{g}(V_d-V_u) \tag{C8}$$

If α is defined by

$$\alpha \equiv \frac{A_u}{A_d} \tag{C9}$$

equation (C8) can be written

$$p_u - p_d = \left(\frac{\alpha}{g}\right)\left(\frac{w_a}{A_u}\right)(V_d-V_u) = \frac{\alpha}{g}(\rho_u V_u)(V_d-V_u) = \frac{\alpha}{g}\rho_u V_u^2\left(\frac{V_d}{V_u} - 1\right)$$

or, by means of equations (C6) and (C9) and rearrangement,

$$1 - \frac{p_d}{p_u} = \frac{\gamma\alpha}{\gamma g\left(\frac{p_u}{\rho_u}\right)} V_u^2\left(\alpha\frac{\rho_u}{\rho_d} - 1\right)$$

by equation (C4),

$$\frac{p_d}{p_u} = 1 + \gamma\alpha M_u^2\left(1 - \alpha\frac{\rho_u}{\rho_d}\right) \tag{C10}$$

Substituting equation (C10) into (C7) and solving the quadratic equation for ρ_u/ρ_d give the following expression:

$$\frac{\rho_u}{\rho_d} = \frac{(1+\alpha\gamma M_u^2) - \sqrt{(1+\gamma\alpha M_u^2)^2 - (\gamma+1)(\alpha M_u)^2\ 2 + (\gamma-1)M_u^2}}{(\gamma+1)(\alpha M_u)^2} \tag{C11}$$

Equation (C11) provides ρ_u/ρ_d and equation (C10) then provides p_d/p_u. (Eq. (C11) requires use of an adequate number of significant figs. to provide accurate results.)

Sudden Contraction: - Isentropic Relation

In contracting to the entrance of the narrow passage the fluid undergoes a shear stress on the face CF (accompanying sketch). If

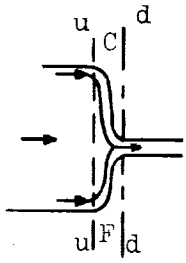

this shear is negligible by comparison with the static pressure decrease, the process is approximately insentropic; hence, before the vena contracta loss downstream of section d-d is experienced,

$$\frac{p_d}{p_u} = \left(\frac{\rho_d}{\rho_u}\right)^{\gamma} \tag{C12}$$

On substituting equation (C12) in (C7), and on defining $\alpha \equiv \frac{A_d}{A_u}$,

$$1 - \left(\frac{\rho_d}{\rho_u}\right)^{\gamma-1} = \frac{\gamma-1}{2} M_u^2 \left[\frac{1}{\alpha^2\left(\frac{\rho_d}{\rho_u}\right)^2} - 1\right] \tag{C13}$$

This equation may be solved graphically for ρ_d/ρ_u, and equation (C12) then provides p_d/p_u. For the cycle calculations, these static pressures were converted to total pressures by use of the standard relations.

APPENDIX D

THERMAL STRESS AND SHOCK

Steady state. - In reference (9) it is shown that the steady-state temperature distribution and the corresponding thermal stress distribution are governed by the parameters $q'''\varepsilon^2/8K_{pe}\theta_S$ and K_{pS}/K_{pe}. The first parameter was obtained as follows: From the heat balance,

$$q'' = h\,(T_S-T_a)$$

and for a heat-generating plate equally cooled on both faces,

$$q''' = q''/\left(\frac{\varepsilon}{2}\right) = 2h\,(T_S-T_a)/\varepsilon$$

Therefore,

$$\frac{q'''\varepsilon^2}{8K_{pe}\theta_S} = \frac{1}{4}\,\frac{h\varepsilon}{K_{pe}}\,\frac{T_S-T_a}{\theta_S}$$

The stress is greatest where $q'''\varepsilon^2/8K_{pe}\theta_S$ has its greatest value, and for a theoretically isothermal reactor surface the greatest value occurs at a short distance beyond reactor inlet. Inasmuch as neither the local value of h nor the local value of T_a was precisely known near the reactor inlet, the average reactor heat-transfer coefficient h_{av} and the inlet-air temperature T_3 were employed as first approximations. The arbitrarily assignable reference temperature T_e, which occurs in the definition

$$\theta_S \equiv T_S-T_e$$

was also assigned the value T_3. Hence,

$$\frac{T_S-T_a}{\theta_S} \simeq \frac{T_S-T_3}{T_S-T_3} = 1$$

and therefore at the reactor inlet, where the severest stresses occur,

$$\frac{q'''\varepsilon^2}{8K_{pe}\theta_S} \simeq \frac{1}{4}\,\frac{h_{av}\varepsilon}{K_{pe}}$$

In evaluating K_{pe} and K_{pS}/K_{pe} of fuel-impregnated plate, the available experimental data (ref. 10) for pure $MoSi_2$ were employed. The thermal conductivity of $MoSi_2$ has been experimentally determined for temperatures from 700° to 1460° R (fig. 14(a)) and it was assumed that the linear variation exhibited in this temperature range could be extrapolated to 1565° R; hence K_{pe} was assumed known for compressor pressure ratios to 25. Stresses were computed for several possible values of K_{pS}/K_{pe}, inasmuch as the actual variation in conductivity of $MoSi_2$ at temperatures substantially higher than 1460° R has not been experimentally determined.

For combinations of values of the parameters $q'''\varepsilon^2/8K_{pe}\theta_S$ and K_{pS}/K_{pe} the dimensionless surface stress, $\sigma_S(1-\nu)/\beta E\theta_S$, was obtained from figure 14(b) of this report; this figure was taken from reference 9. The actual stress was then obtained by assuming that fuel-impregnated $MoSi_2$ has the same physical properties as pure $MoSi_2$, that is, $E = 56\times10^6$ pounds per square inch, $\nu \cong 0.3$, and $\beta = 5.4\times10^{-6}\ {}^{\circ}R^{-1}$.

Thermal shock. - In (ref. 9) it is shown that the transient temperatures and thermal stresses in a heat-generating plate of linearly variable conductivity are governed by the initial temperature distribution (that is by $q'''\varepsilon^2/8K_{pe}\theta_S$ and K_{pS}/K_{pe}) and by the parameters $h\varepsilon/2K_{pe}$, K_{pS}/K_{pe}, and the Fourier number. It was assumed, for lack of precise information, that in the reactor inlet region the air temperature in the first fractions of a second after emergency shut-down would not differ much from the original steady-state value, and T_e was taken equal to T_3. Thus K_{pS}/K_{pe} in the transient state was assumed to be the same as in the steady state. It was also assumed that the heat-transfer coefficient in the first instants of the transient state was the same as in the original steady state; hence, $h\varepsilon/2K_{pe}$ was the same for the transient and steady states. If these assumptions do not differ much from the realities, it follows from reference 9 that the maximum transient stress will occur at the instant of immersion, and will not differ substantially from the maximum steady-state stress. Reactor after-heat would help minimize any tendencies toward shock.

REFERENCES

1. Anon.: Aircraft Nuclear Propulsion Project: Engineering Progress Report No. 2. DC-51-12-25, Aircraft Gas Turbine Dept., General Electric Co., Oct. 1, 1951-Dec. 31, 1951. (USAF Contract AF33(038)-21102; USAEC Contract AT(11-1)-171). December 1951.

2. Humble, Leroy V., Lowdermilk, Warren H., and Desmon, Leland G.: Measurements of Average Heat-Transfer and Friction Coefficients for Subsonic Flow of Air in Smooth Tubes at High Surface and Fluid Temperatures. NACA Rep. 1020, 1951.

3. Keenan, Joseph H., and Kaye, Joseph: Thermodynamic Properties of Air. John Wiley Sons, Inc., 1945.

4. Glassman, Irvin, and Bonilla, Charles F.: Thermal Conductivity and Prandtl Number of Air at High Temperatures. Preprint, Heat Transfer Symposium, Forty-Fourth Annual Meeting American Institute of Chemical Engineers, December 1951.

5. Wood, George P., and Brevoort, Maurice J.: Design, Selection, and Installation of Aircraft Heat Exchangers. NACA WR L-341, 1943. (Supersedes NACA ARR 3G31.)

6. Anon.: Flow of Fluids through Valves, Fittings, and Pipe. Tech. Paper No. 409, Eng. and Res. Div., Crane Co., May 1942.

7. Henry, John R.: Design of Power-Plant Installations Pressure-Loss Characteristics of Duct Components. NACA WR L-208, 19 NACA ARR L4F26, June 1944.

8. Anon.: Fluid Meters, Their Theory and Application. A.S.M.E. Res. Pub., Pub. by Am. Soc. Mech. Eng. (New York), 4th ed., 1937, pp. 35, 37.

9. Manson, S. V.: Temperatures, Thermal Stress, and Shock in Heat-Generating Plates of Constant and of Linearly Varying Thermal Conductivity.

10. Long, Roger A.: Fabrication and Properties of Hot-Pressed Molybdenum Disilicide. NACA RM E50F22, 1950.

11. Anon.: NACA Conference on Aircraft Propulsion Systems Research, Jan. 18-19, 1950.

12. Kulakowski, J. L., Kaler, G. M., and Grogan, G. C.: Generalized Lift and Drag Characteristics at Subsonic, Transonic, and Supersonic Speeds. Consolidated Vultee Report. FZA - 041a, 1950.

13. de Karman, Th.: The Problem of Resistance in Compressible Fluids. Quinto Convegno "Volta," Reale Accademia d'Italia (Roma), Sett. 30- Ott. 6, 1935, pp. 3-57.

14. The Staff of the Ames 1- by 3-Foot Supersonic Wind-Tunnel Section: Notes and Tables for Use in the Analysis of Supersonic Flow. NACA TN 1428, 1947.

15. Vidal, Robert J., and Loy, Ramond E.: Projected Capabilities of Nuclear Powered Airplanes. II. Application to a Supersonic Airplane (Mach Number = 1.5). Fairchild Engine and Airplane Corporation. NEPA 1724, 1951.

16. Wachtl, William W., and Rom, Frank E.: Analysis of the Liquid-Metal Turbojet Cycle for Propulsion of Nuclear Powered Aircraft. NACA RM E51D30, 1951.

17. Marks, Lionel S.: Mechanical Engineer's Handbook. McGraw-Hill Book Co., Inc., 1941.

TABLE I - TABULATION OF OPTIMUM PERFORMANCE

	Case II		Case III		
	A	B	A	B	C
Reactor fuel plate surface temperature T_s, $^{\circ}R$	2,660	2,660	2,960	2,960	2,960
Turbine-inlet temperature T_5, $^{\circ}R$	2,000	2,000	2,600	2,600	2,600
Reactor fuel element thickness ϵ, in.	.07	.01	.01	.07	.01
Compressor pressure ratio P_2/P_1	15	15	15	15	25
Reactor free flow ratio α	0.40	0.50	0.49	0.36	0.49
Reactor diameter d_R, ft	8.5	8.0	5.0	5.5	4.0
Reactor length l_R, ft	3.14	3.28	4.05	4.10	4.00
Pressure ratio across reactor and shields P_5/P_2	0.760	0.785	0.725	0.661	0.770
Air flow per reactor frontal area w_a/A_R, lb/sec-ft^2	50.0	50.8	48.1	45.0	77.5
Total engine air flow w_a, lb/sec	2,836	2,550	960	1,066	974
Total net thrust F_n, lb	81,000	75,000	53,000	57,000	48,800
Length of nose cone section l_x, ft	75.0	73.8	67.8	70.0	60.8
Length of nose straight section $l_{x,1}$, ft	21.4	23.0	31.7	24.4	38.8
Length of main body section l_y, ft	27.2	27.0	25.1	25.3	24.9
Length of boattail section l_z, ft	52.3	53.5	65.1	64.9	57.4
Total length of fuselage l_F, ft	175.9	177.3	189.7	184.6	182.0
Diameter of nose section d_x, ft	12.5	12.3	11.3	11.7	10.1
Diameter of main body d_F, ft	16.3	15.8	12.8	13.3	11.8
Diameter of jet nozzle exit d_0, ft	11.2	10.5	6.3	6.9	6.2
Drag of nose cone section D_x, lb	4,980	4,825	4,075	4,350	3,275
Drag of nose straight section $D_{x,1}$, lb	1,648	1,738	2,200	1,748	2,415
Drag of main body section D_y, lb	2,515	2,418	1,825	1,905	1,670
Drag of boattail section D_z, lb	7,940	7,720	6,180	6,564	5,180
Total drag of fuselage D_F, lb	17,083	16,701	14,280	14,567	12,540
Weight of engine shafts, lb	16,350	15,270	8,500	9,200	10,250
Weight of engines W_{c+T}, lb	65,800	58,800	18,500	21,200	21,750
Total shield plus reactor weight, lb	184,850	170,460	123,500	136,100	110,500
Weight of auxiliary equipment, lb	32,000	32,000	32,000	32,000	32,000
Weight of structure W_s, lb	181,500	165,470	109,000	119,500	104,500
Total airplane gross weight W_g, lb	480,500	442,000	291,500	318,000	279,000
Total reactor heat release Q, Btu/sec	504,000	449,000	332,000	370,500	284,000
Airplane lift-drag ratio L/D	5.93	5.89	5.52	5.58	5.60
Maximum thermal stress in fuel plates for extremes of assumed thermal conductivity, lb/in^2	6,000 to 21,600	700 to 2,320	1,000 to 7,200	8,500 to > 40,000	1,500 to 9,500

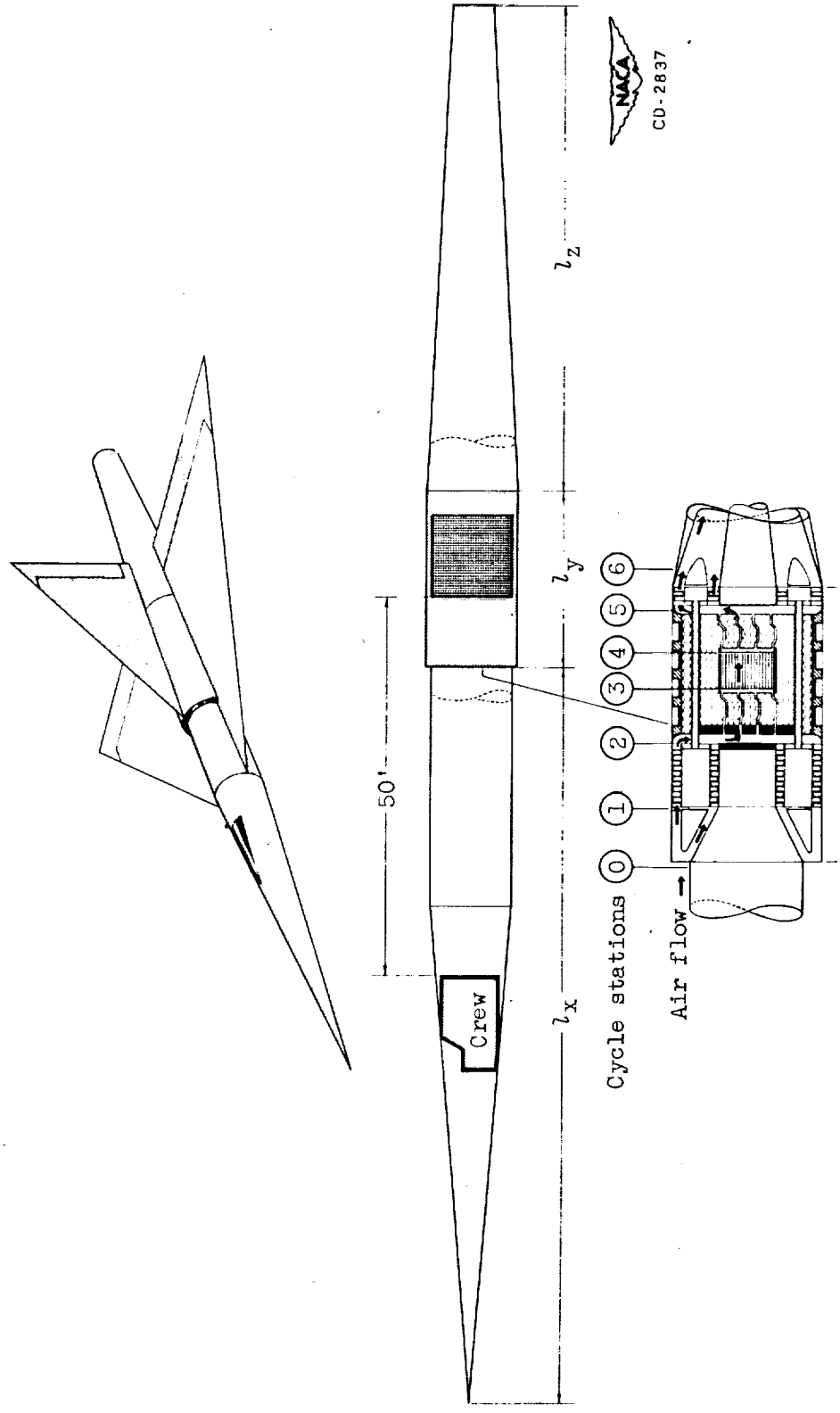

Figure 1. - Schematic diagram of external and internal configurations of direct-air-cycle aircraft.

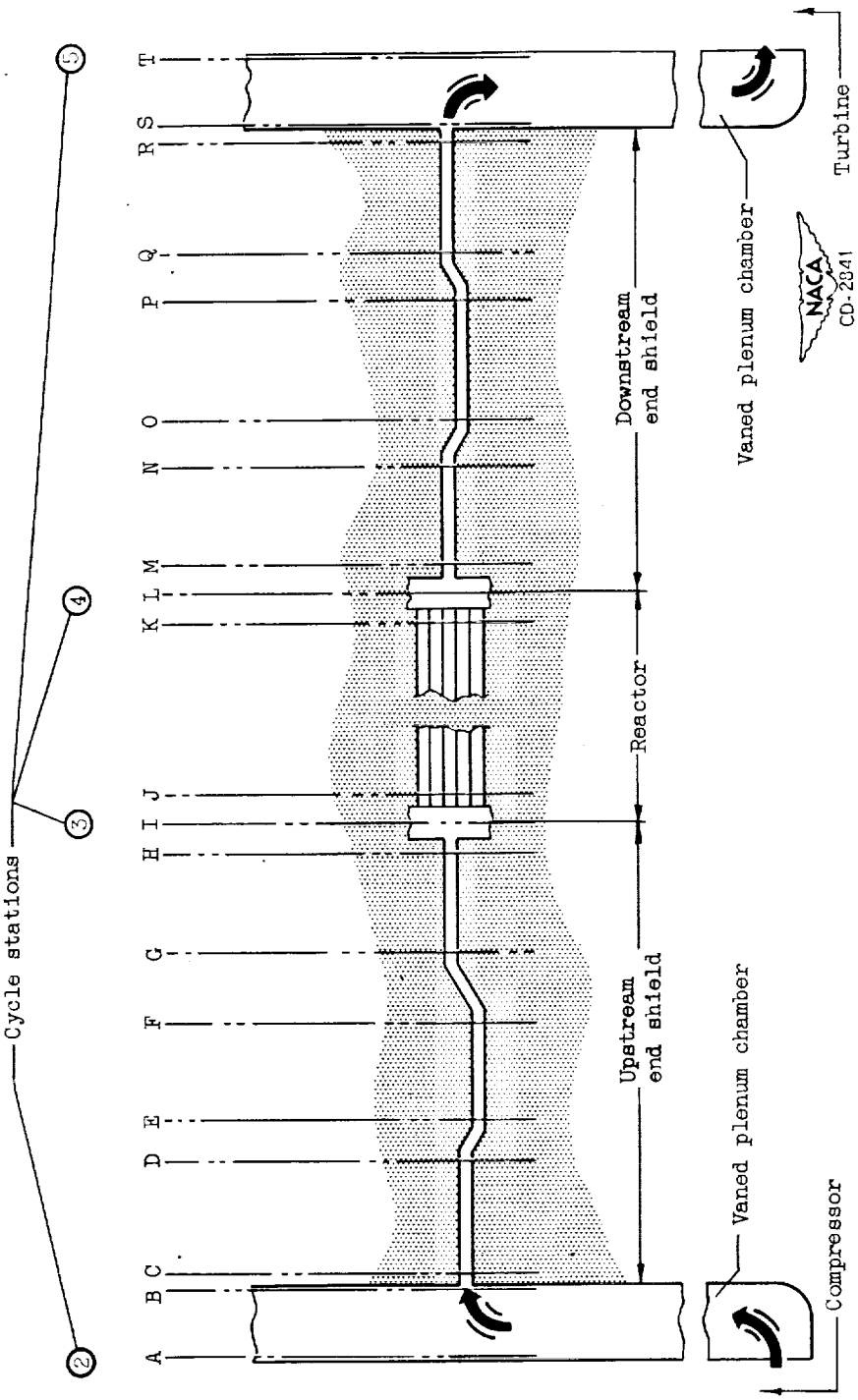

Figure 2. - Schematic diagram of air flow path from compressor exit to turbine inlet, through vaned plenum chambers, end shields, and reactor.

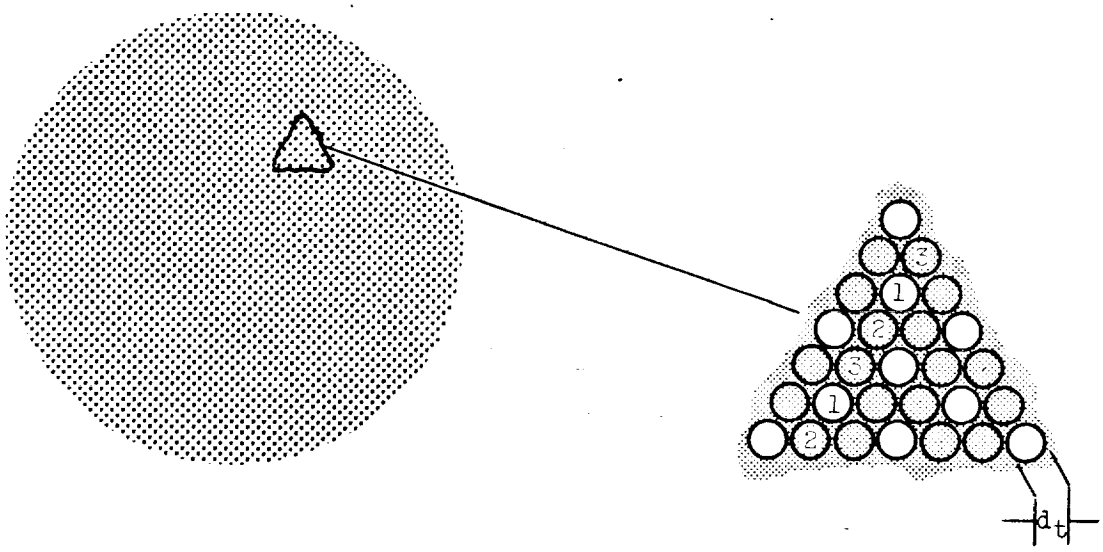

Face of upstream shield

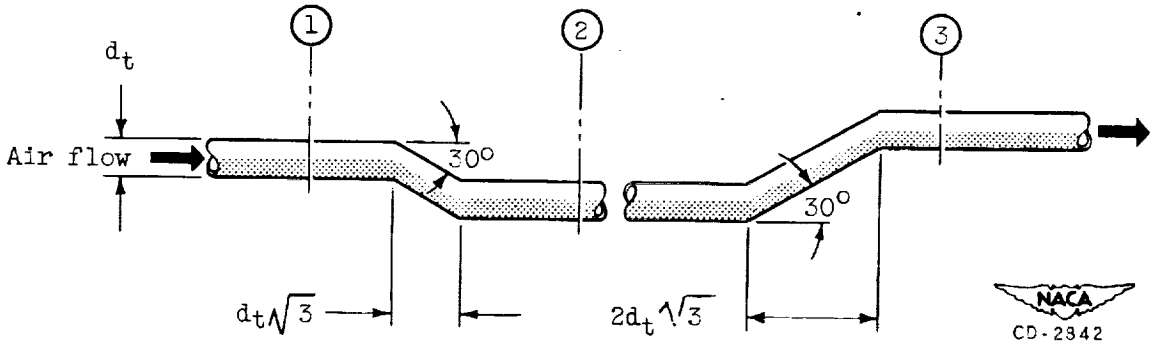

Bend details in axial shield tubes

Figure 3. - Air flow passage detail of end shield (section A of fig. 2).

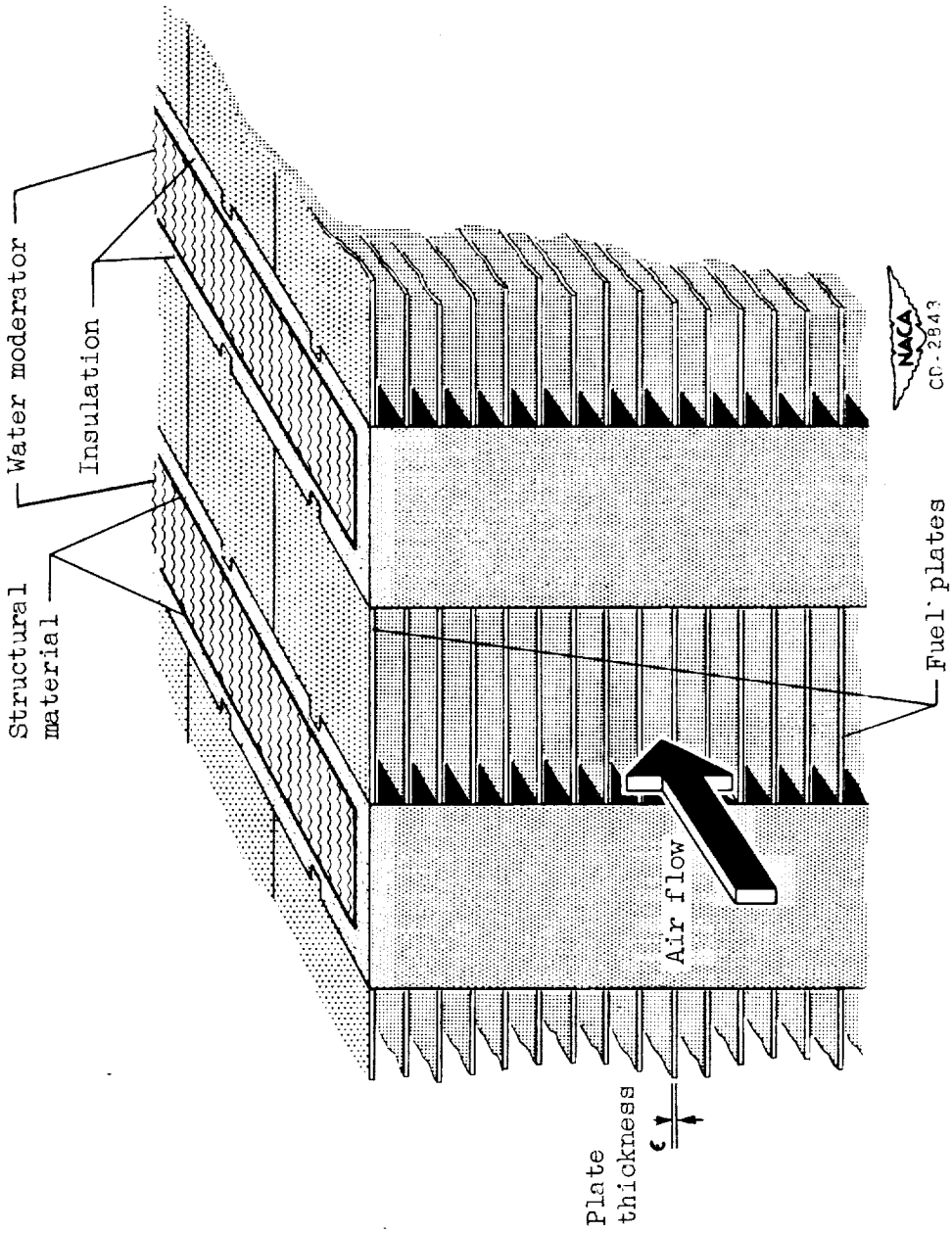

Figure 4. - Schematic arrangement of reactor fuel plates, moderator, and structural material.

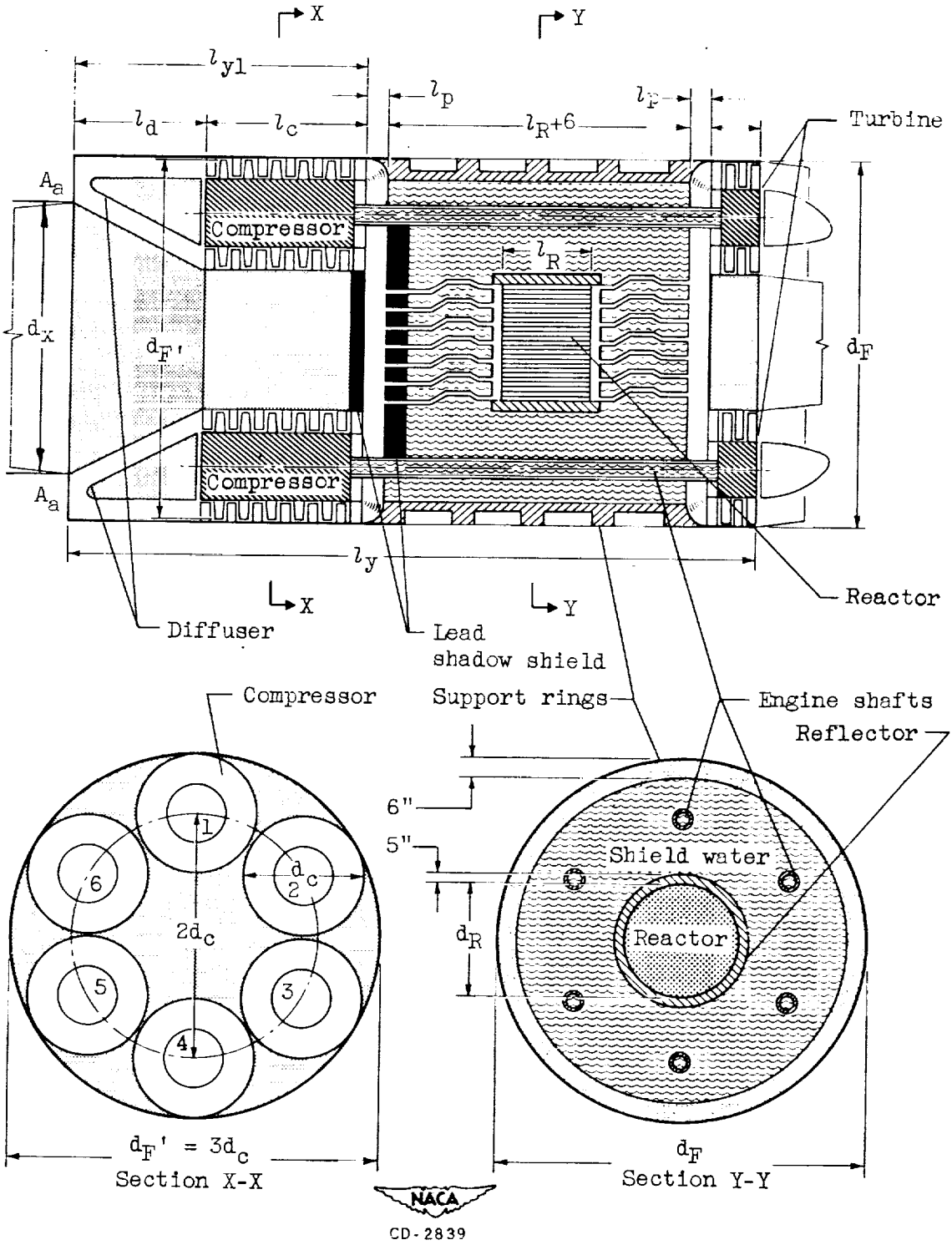

Figure 5. - Schematic view of main body section showing arrangement of engines, shafts, shields, and inlet diffuser, and dimensions of main section.

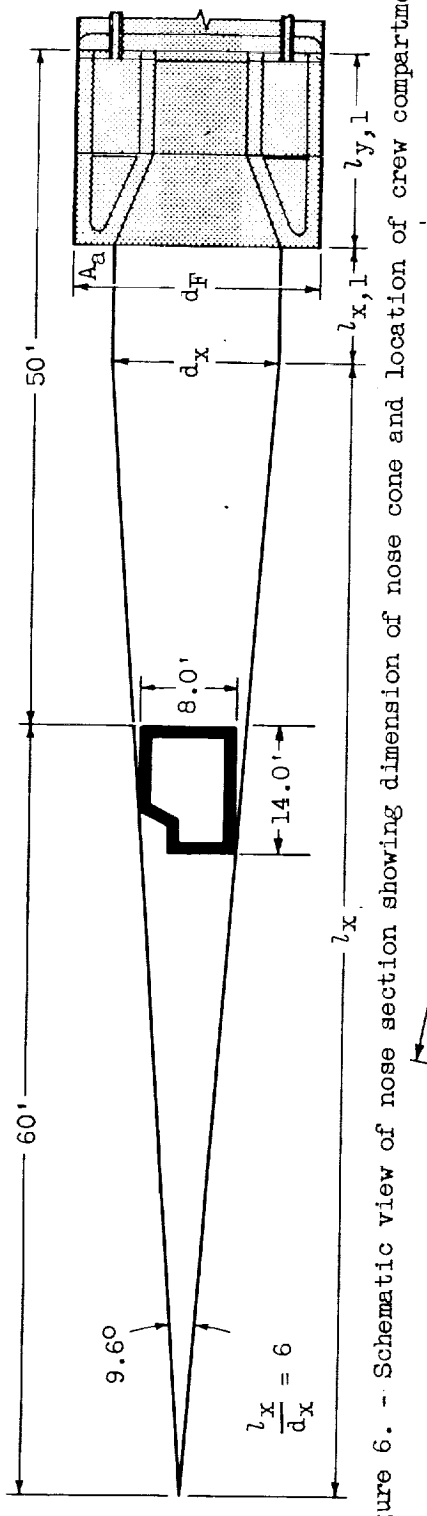

Figure 6. - Schematic view of nose section showing dimension of nose cone and location of crew compartment.

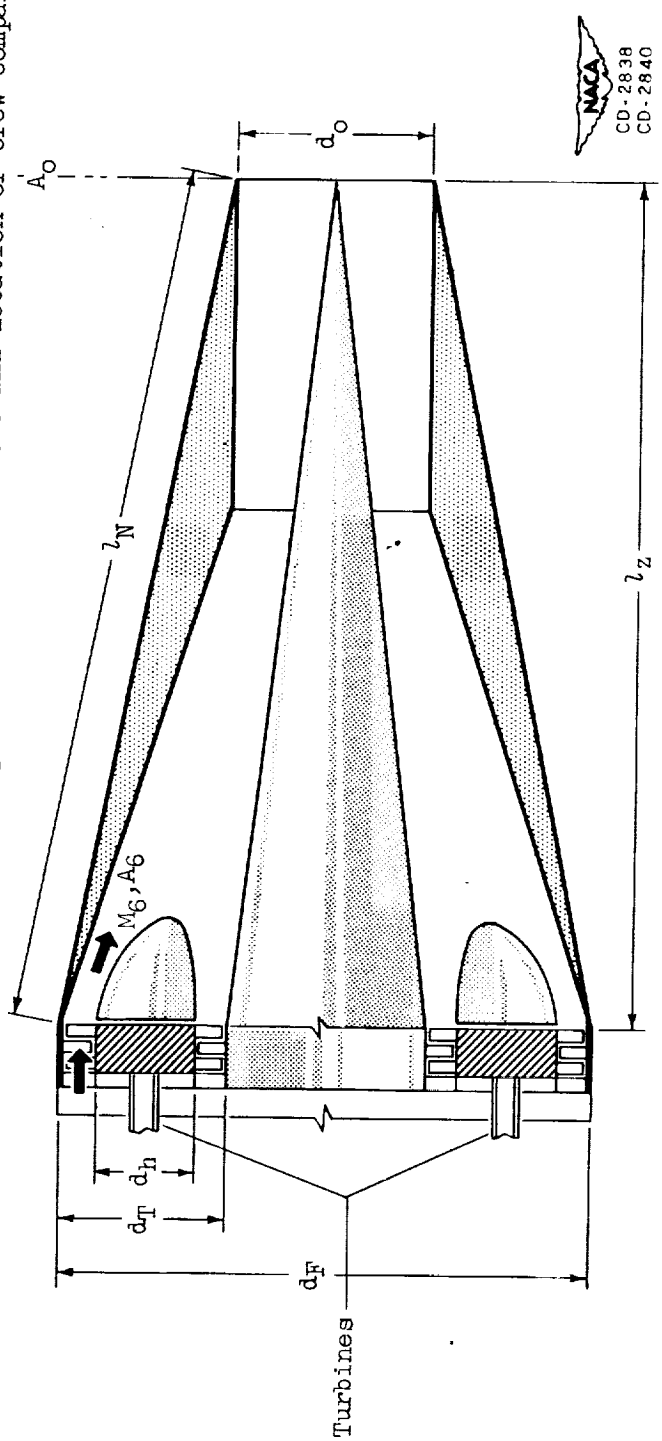

Figure 7. - Schematic view of boattail section showing arrangement and dimensions of exhaust nozzle.

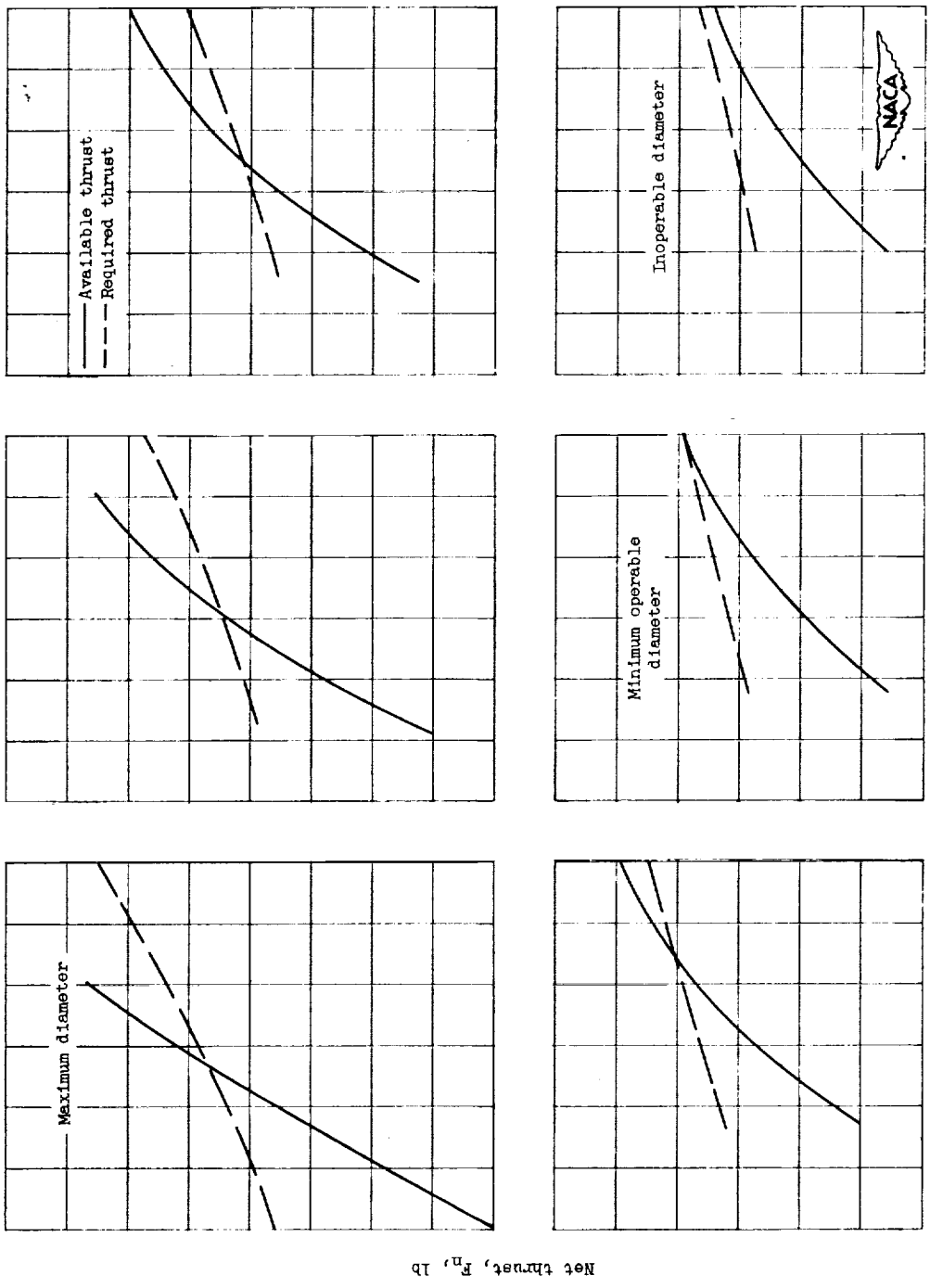

Figure 8. - Curves of available and required F_n as functions of w_a/A_R for several values of d_R illustrating method of solution of thrust-drag equation for a decreasing sequence of six reactor diameters.

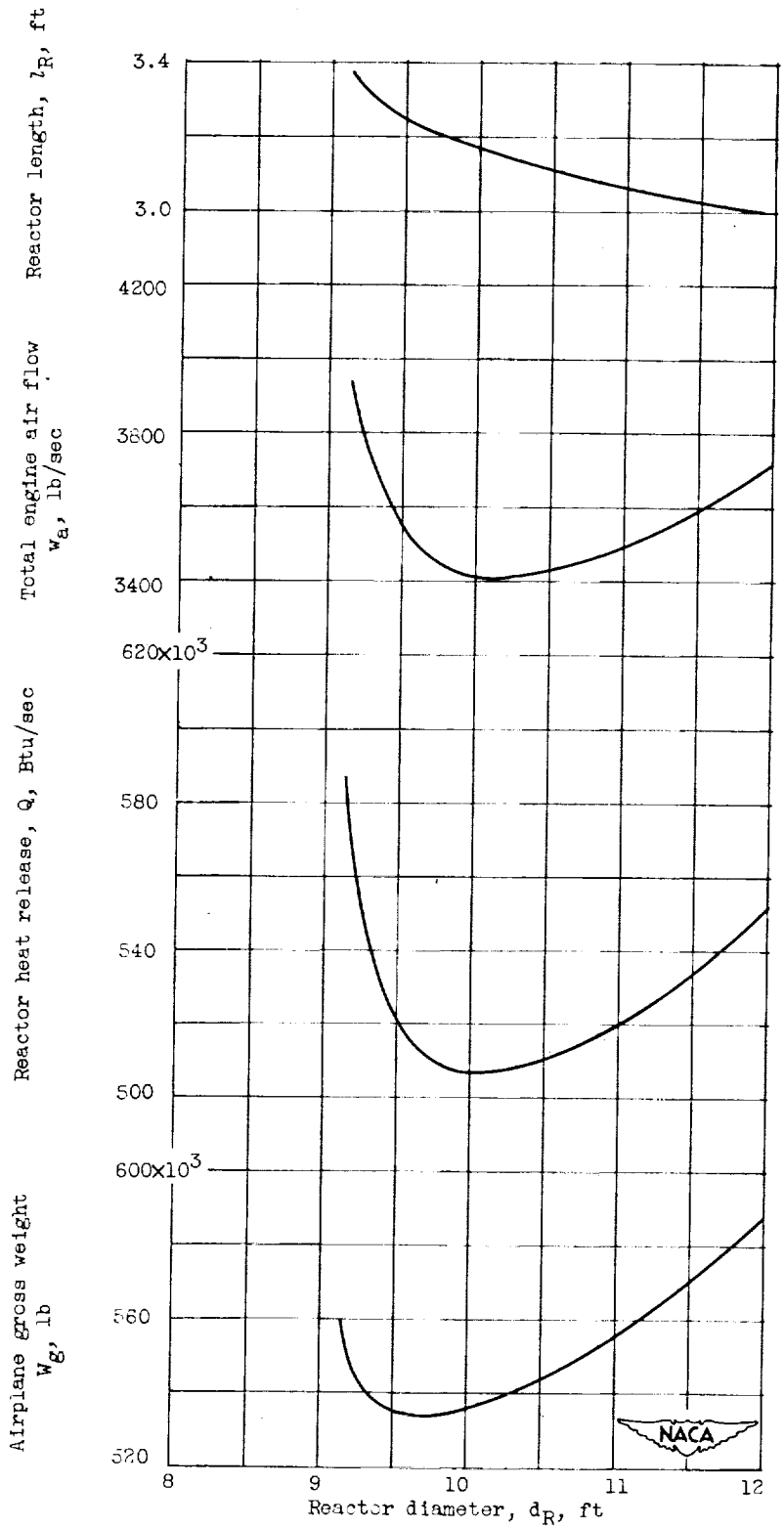

Figure 9. - Curves of W_g, Q, w_a, and l_R as functions of d_R. T_S, 2060° R; T_5, 1900° R; P_2/P_1, 15; ϵ, 0.01 inch; α, 0.49.

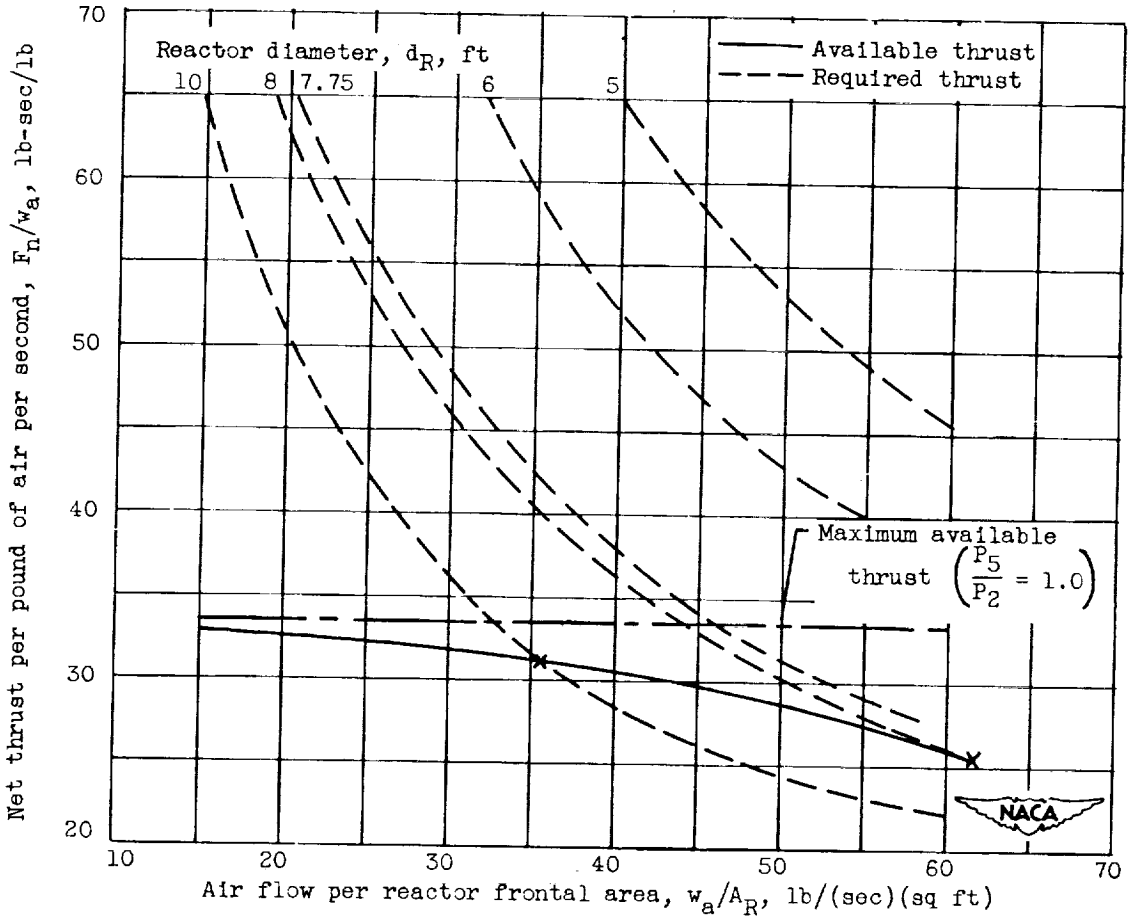

Figure 10. - Curves of available and required F_n/w_a as functions of w_a/A_R for several values of d_R. Case IIA: T_S, 2660° R; T_5, 2000° R; P_2/P_1, 15; ε, 0.07 inch; α, 0.40.

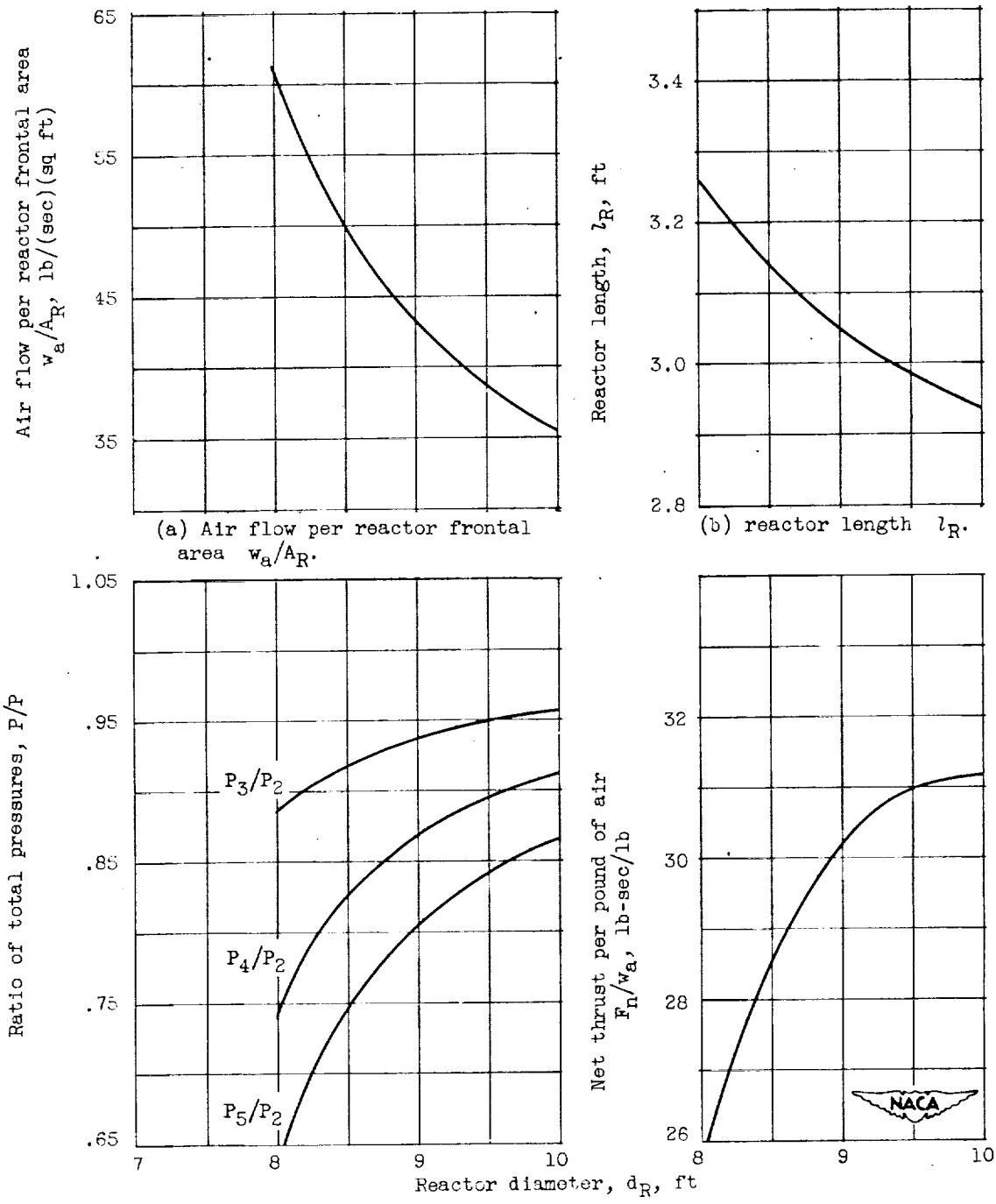

(a) Air flow per reactor frontal area w_a/A_R.

(b) reactor length l_R.

(c) Pressure ratio at several stations of internal flow path.

(d) Net thrust per pound of air per second F_n/w_a.

Figure 11. - Performance parameters as functions of d_R. Case IIA: T_S, 2660° R; T_5, 2000° R; P_2/P_1, 15; ϵ, 0.07 inch; α, 0.40.

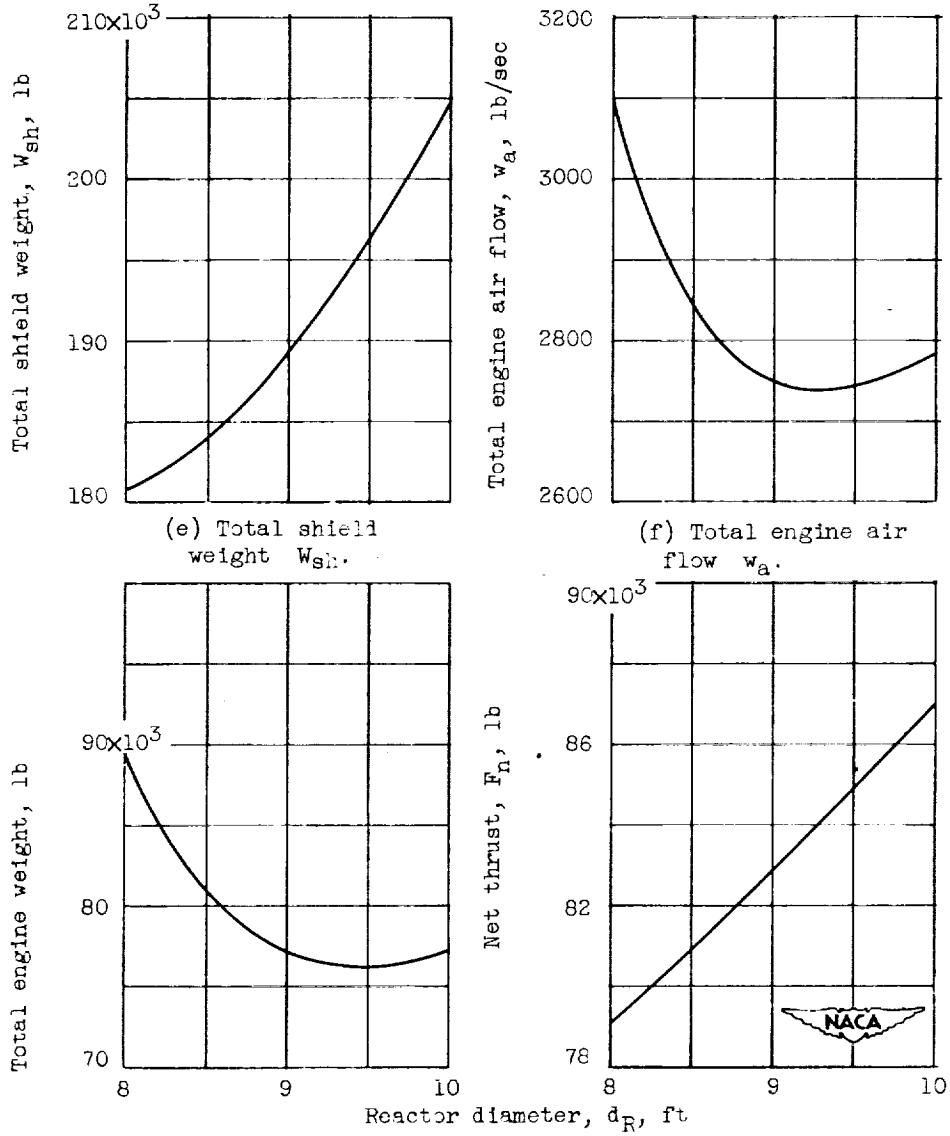

(e) Total shield weight W_{sh}.

(f) Total engine air flow w_a.

(g) Total engine weight.

(h) Total engine thrust F_n.

Figure 11. - Concluded. Performance parameters as functions of d_R.
Case IIA: T_S, 2660° R; T_5, 2000° R; P_2/P_1, 15; ϵ, 0.07 inch; α, 0.40.

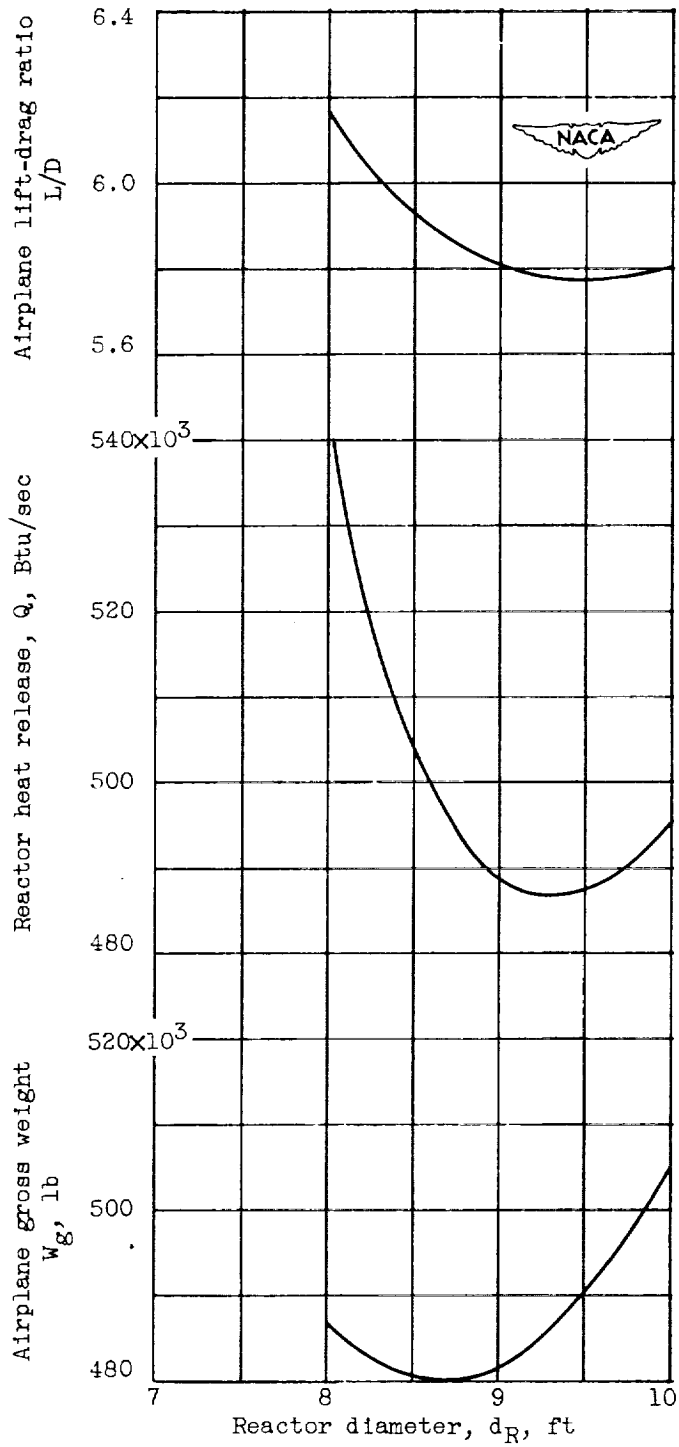

Figure 12. - Curves of W_g, Q, and airplane L/D as functions of d_R. Case IIA: T_S, 2660° R; T_5, 2000° R; P_2/P_1, 15; ε, 0.07 inch; α, 0.40.

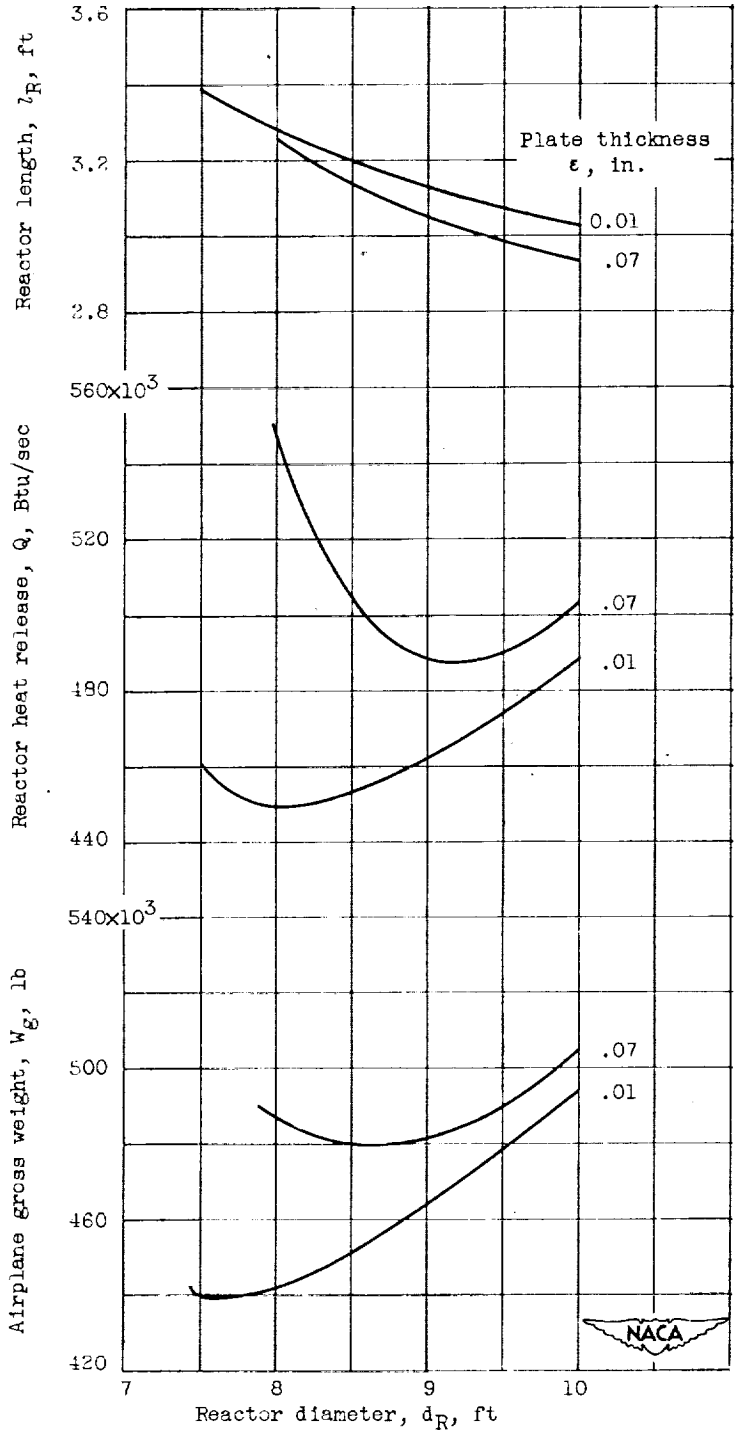

Figure 13. - Curves of W_g, Q, and airplane L/D as functions of d_R. Case II: T_S, 2660° R; T_5, 2000° R; P_2/P_1, 15. Case IIA: ϵ, 0.07 inch; α, 0.40. Case IIB: ϵ, 0.01 inch; α, 0.49.

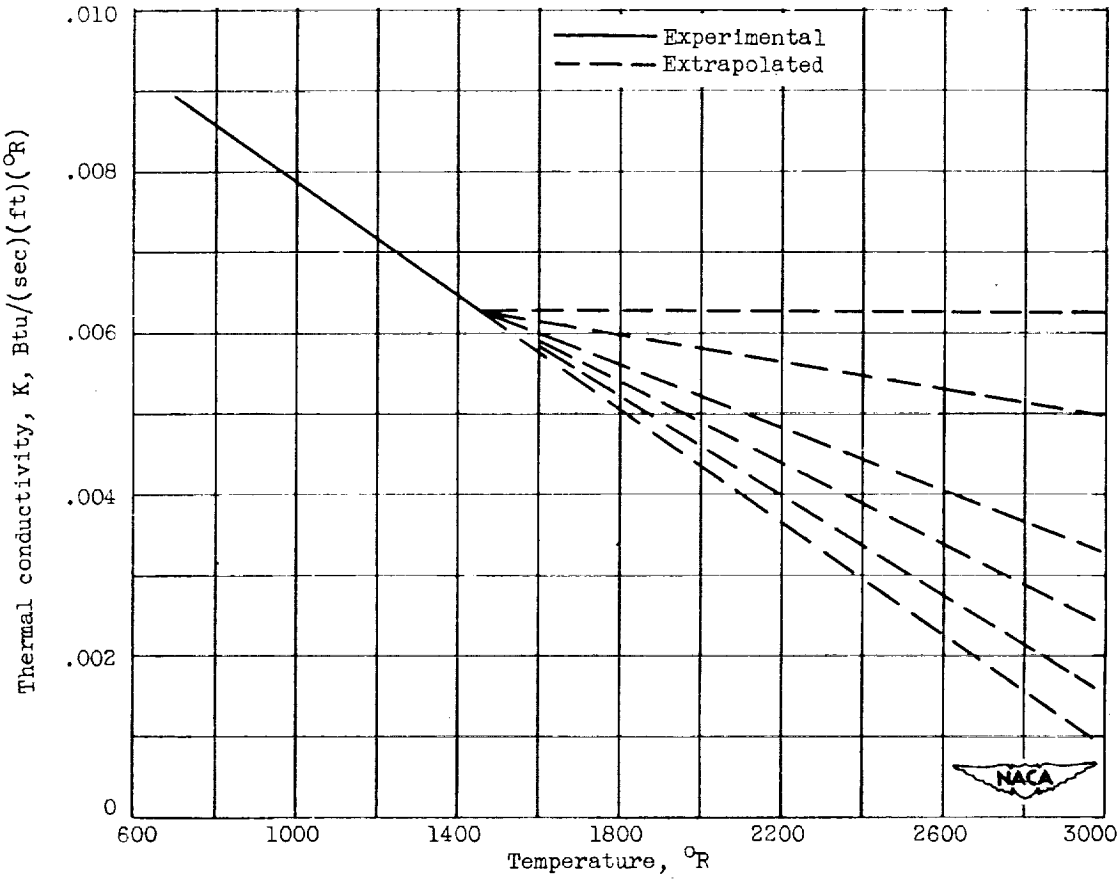

(a) Thermal conductivity of $MoSi_2$ as a function of temperature.

Figure 14. - Curves for determining stress in fuel plates.

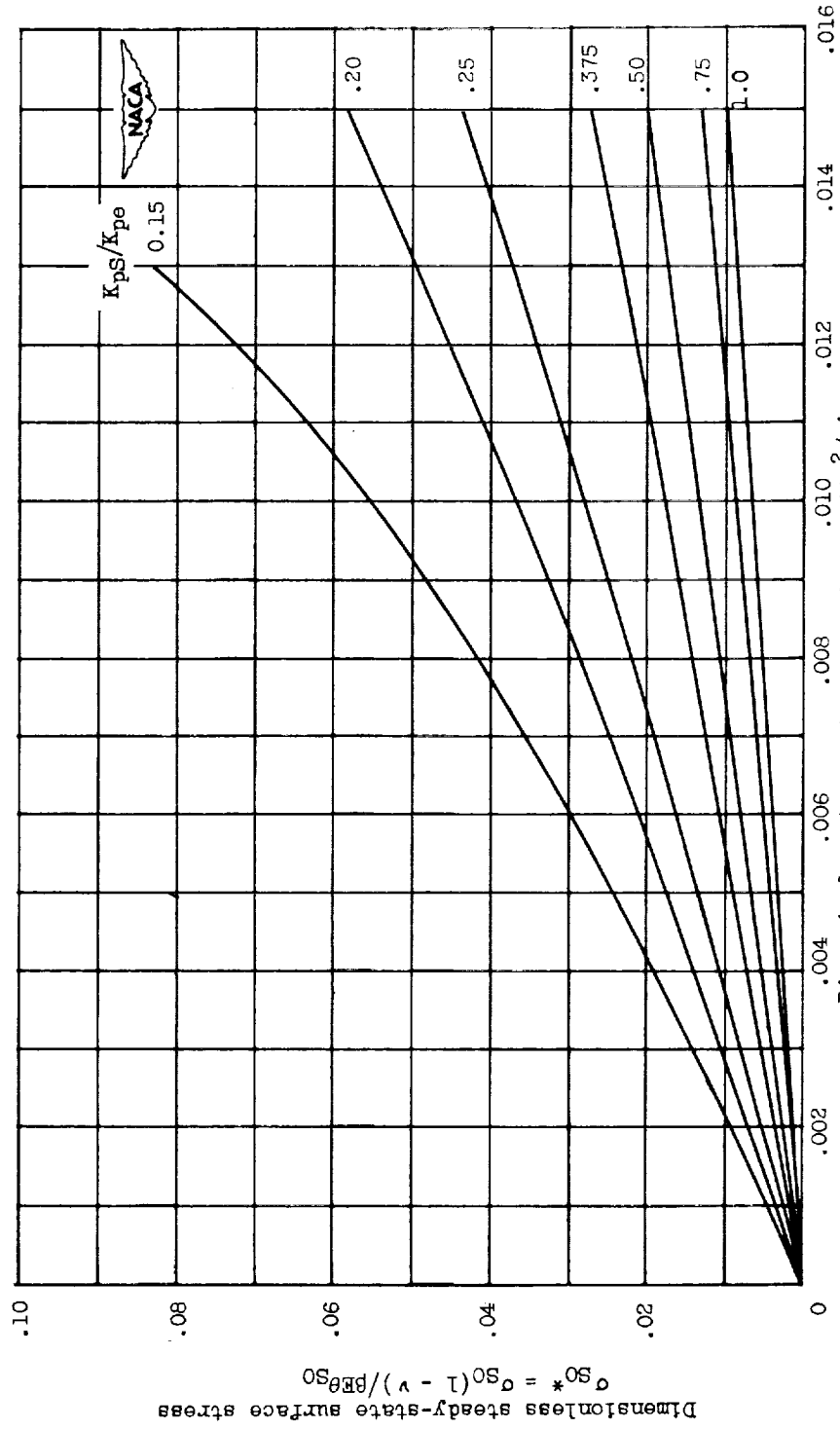

(b) Curves of σ_{SO}^* as a function of $q'''\epsilon^2/8 K_{pe}\theta_{SO}$ for heat-generating plates of linearly varying, and of constant, thermal conductivity.

Figure 14. - Concluded. Curves for determining stress in fuel plates.

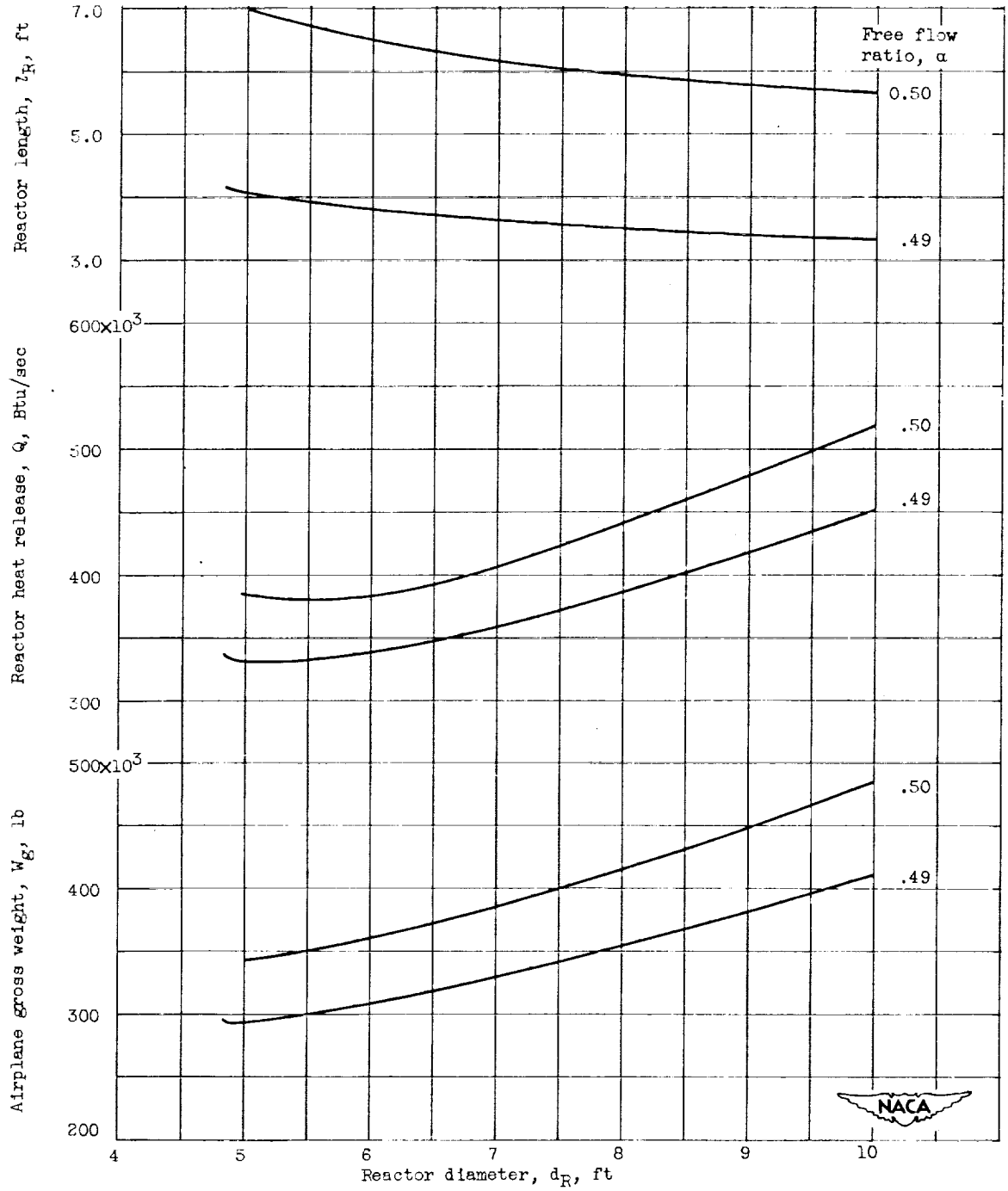

Figure 15. - Effect of α on l_R, W_g, and Q as a function of d_R. T_5, 2600° R; P_2/P_1, 15. Case IIIA: T_S, 2960° R; ϵ, 0.01 inch.

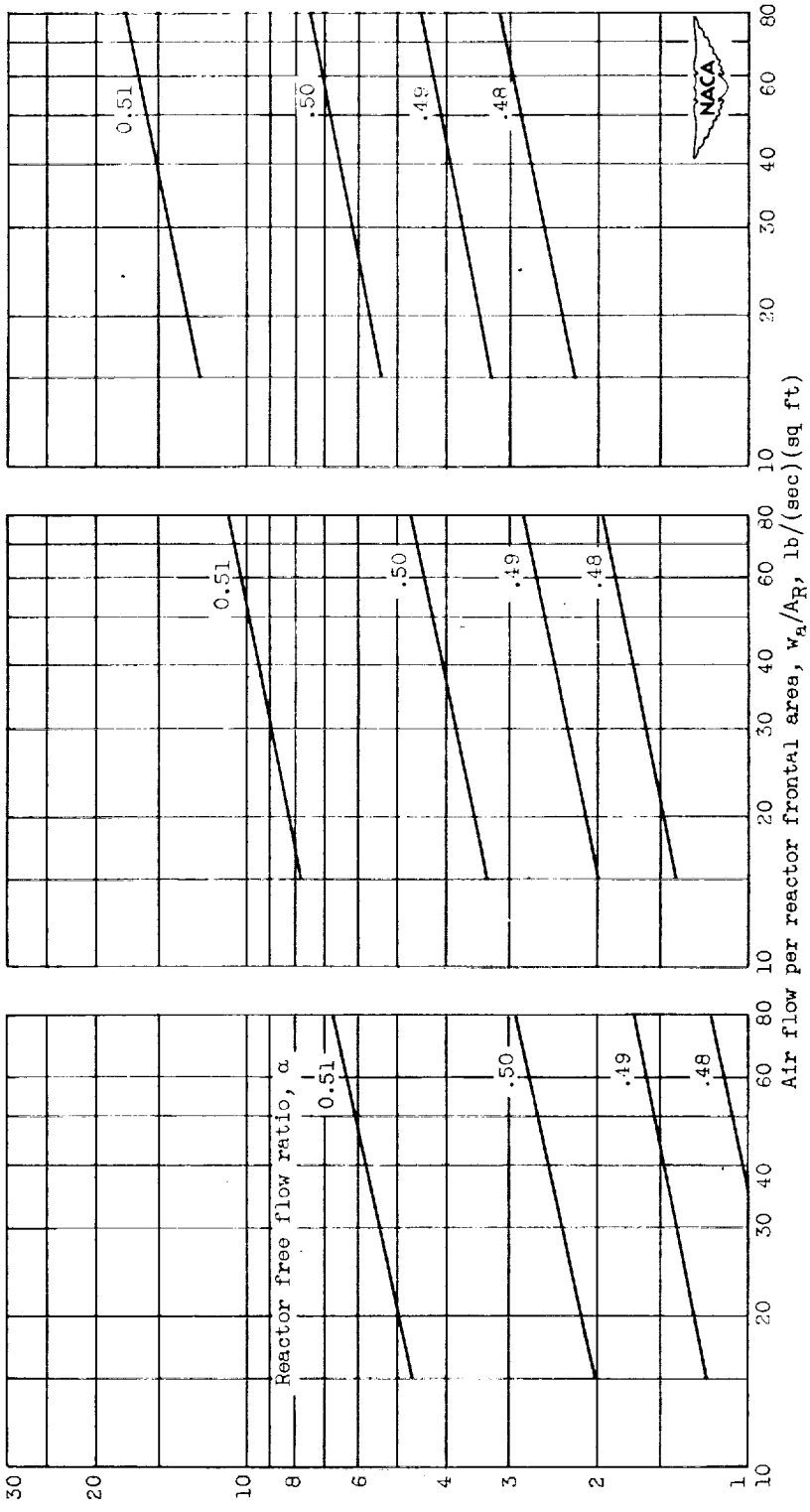

(a) T_5, 2000° R; P_2/P_1, 15.

(b) T_5, 2300° R; P_2/P_1, 15.

(c) T_5, 2600° R; P_2/P_1, 15.

Figure 16. - Curves of l_R as a function of w_a/A_R and T_5 for several values of α. Case IIIA: T_5, 2960° R; ε, 0.01 inch.

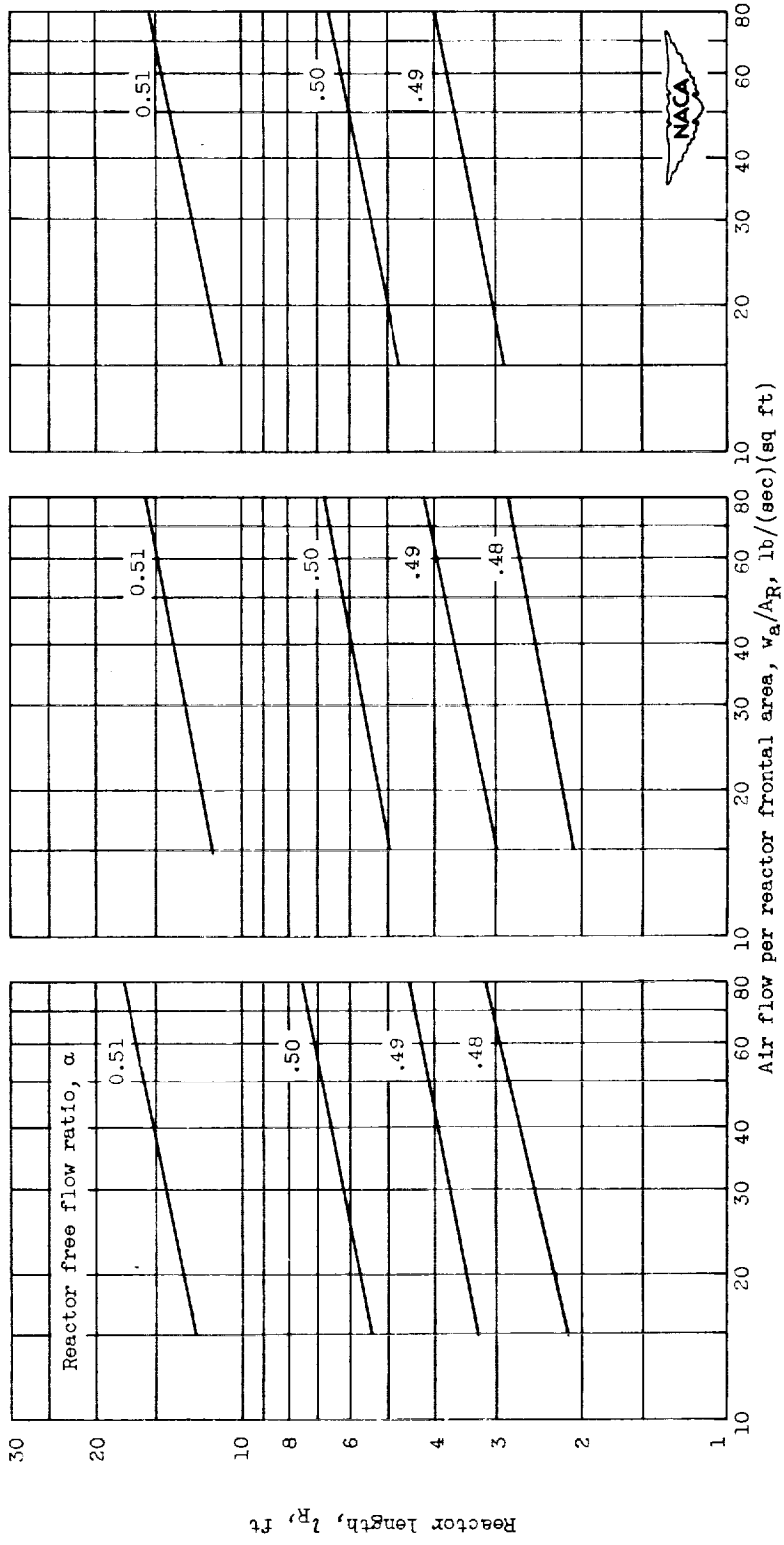

(a) P_2/P_1, 15; T_5, 2600° R. (b) P_2/P_1, 20; T_5, 2600° R. (c) P_2/P_1, 25; T_5, 2600° R.

Figure 17. - Curves of l_R as a function of w_a/A_R and P_2/P_1 for several values of α. Case IIIA: T_5, 2960° R; ε, 0.01 inch.

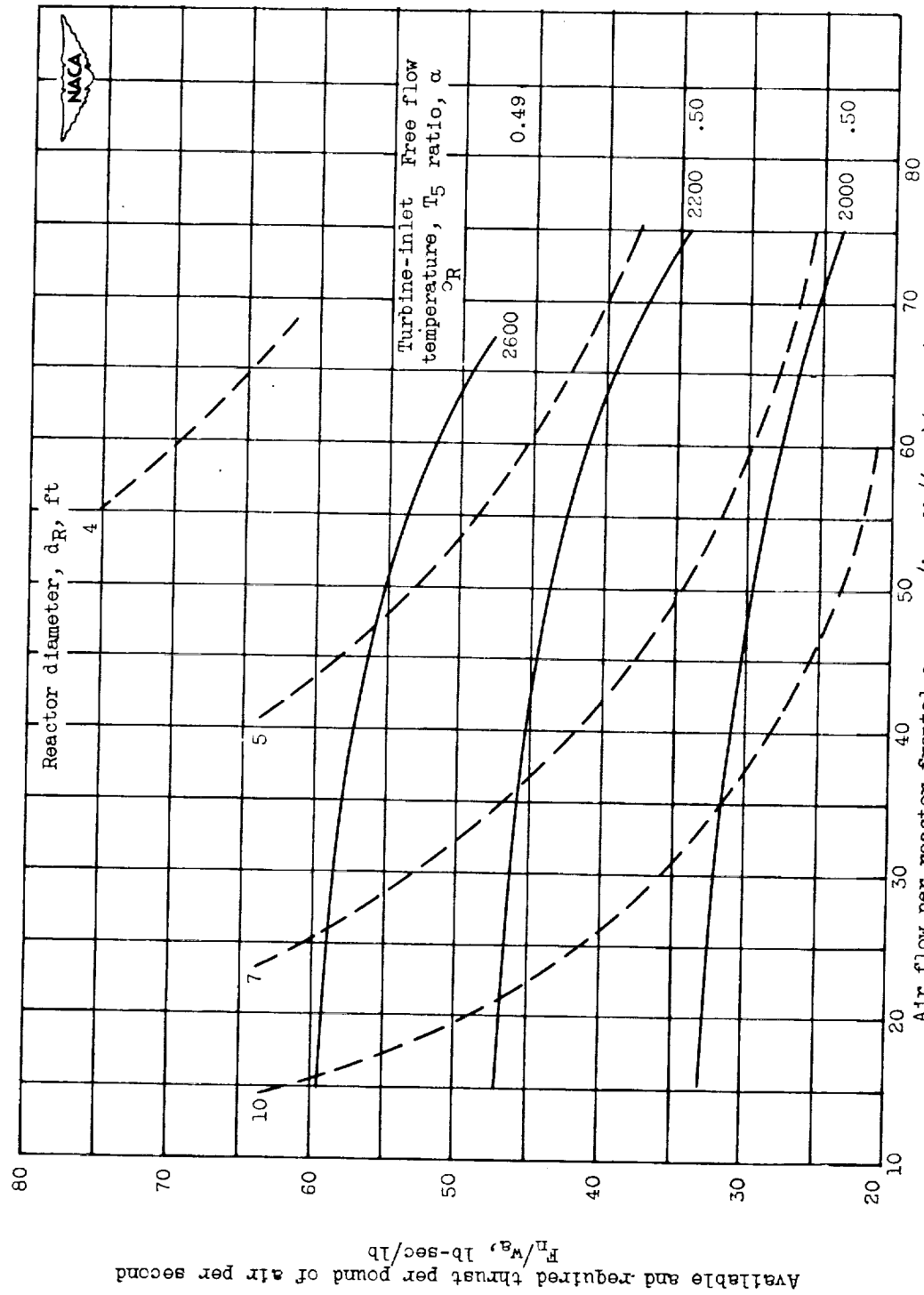

Figure 18. - Curves of available and required F_n/w_a as functions of w_a/A_R for several values of d_R, T_5, and α. P_2/P_1, 15. Case IIIA: T_S, 2960° R; ε, 0.01 inch.

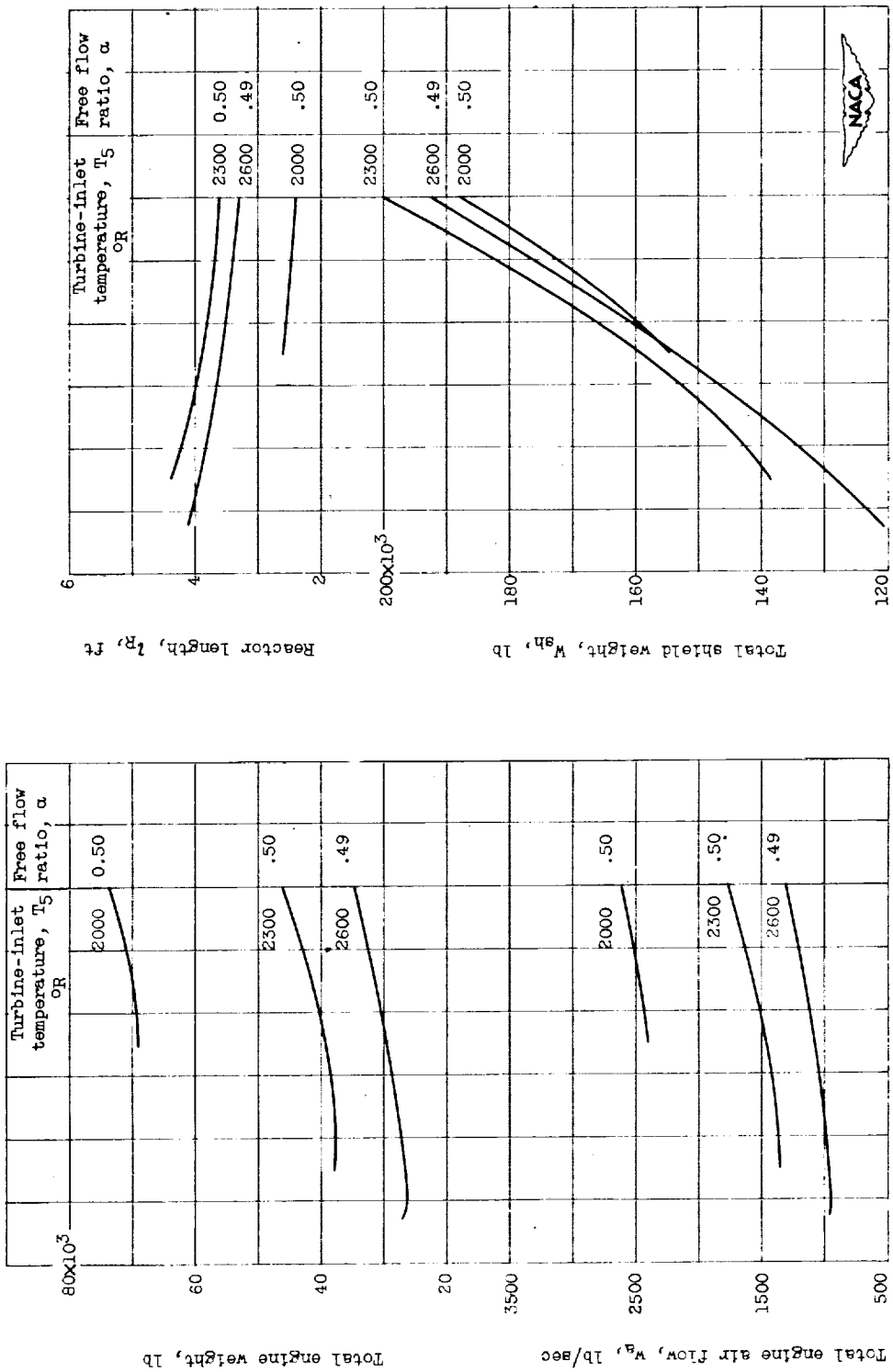

(a) Performance parameters.

Figure 19. - Performance as a function of d_R for several values of T_5 and α. P_2/P_1, 15. Case IIIA: T_5, 2960° R; ε, 0.01 inch.

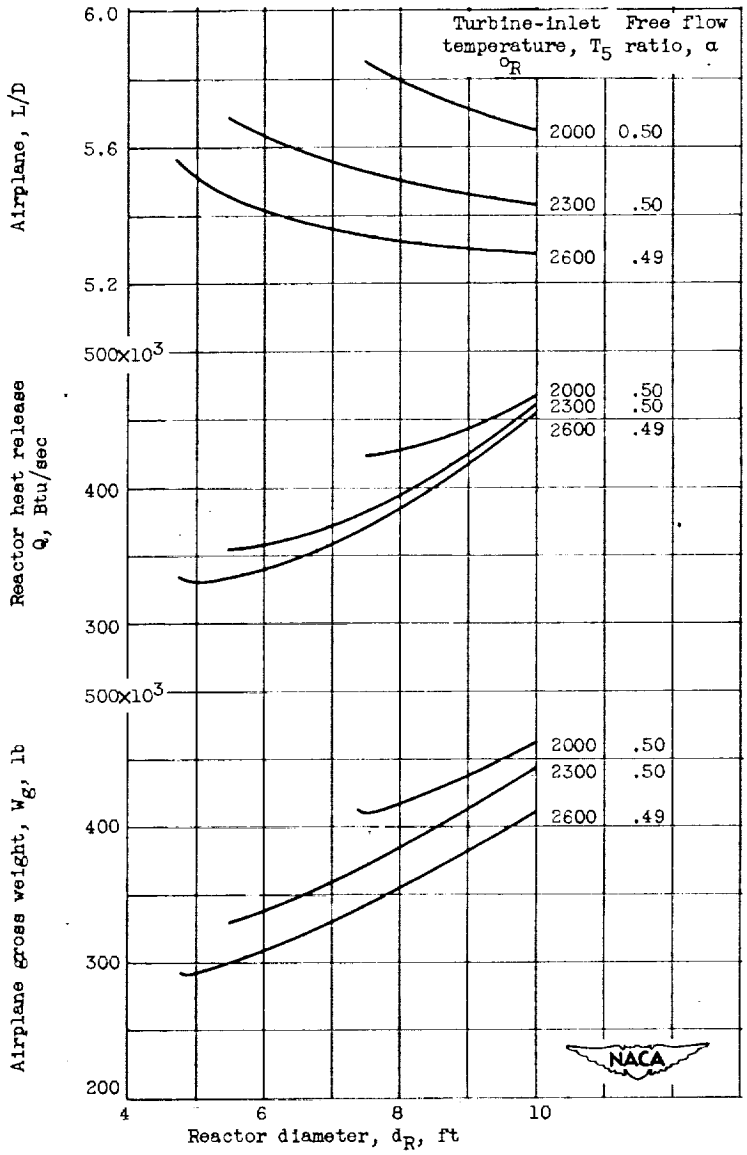

(b) W_g, Q, and airplane L/D.

Figure 19. - Concluded. Performance as a function of d_R for several values of T_5 and α. P_2/P_1, 15. Case IIIA: T_S, 2960° R; ε, 0.01 inch.

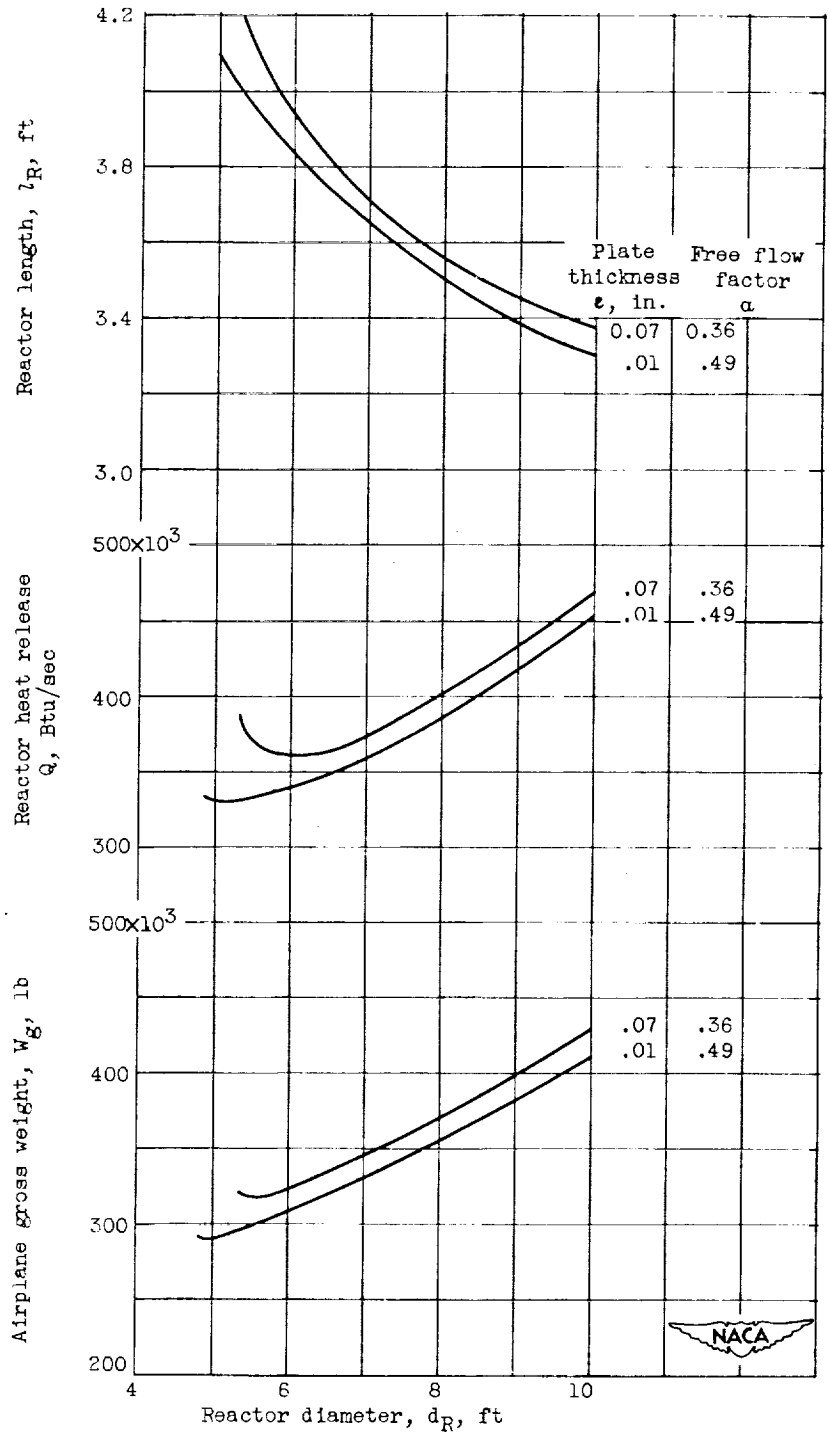

Figure 20. - Effect of ε on W_g, Q, and l_R as a function of d_R. Case III: T_S, 2960° R; T_5, 2600° R; P_2/P_1, 15. Case IIIA: ε, 0.01 inch; α, 0.49. Case IIIB: ε, 0.07 inch; α, 0.36.

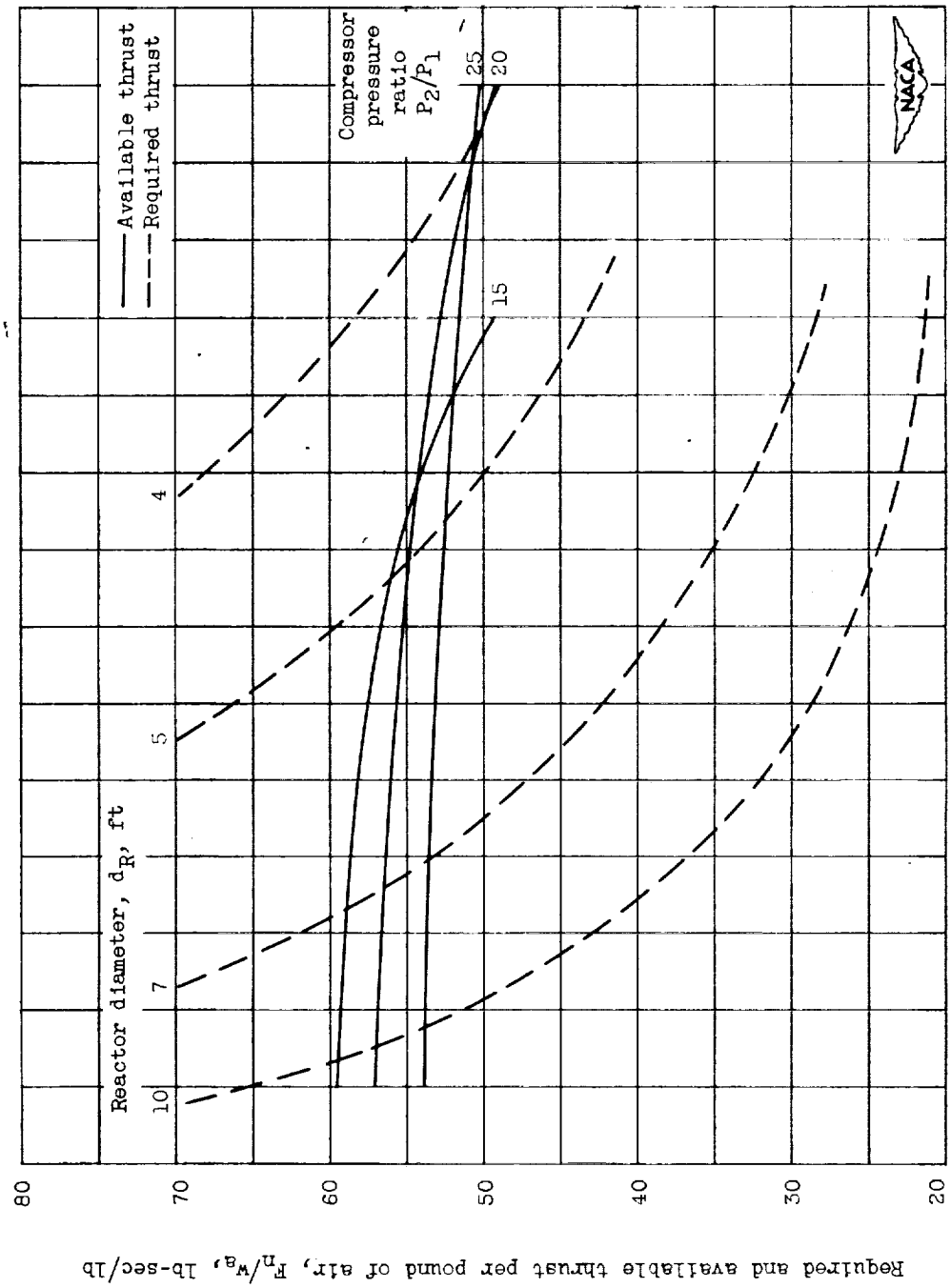

Figure 21. - Curves of available and required F_n/w_a as functions of w_a/A_R for several values of d_R and P_2/P_1. T_5, 2600° R; α, 0.49. Case III: T_5, 2960° R; ϵ, 0.01 inch.

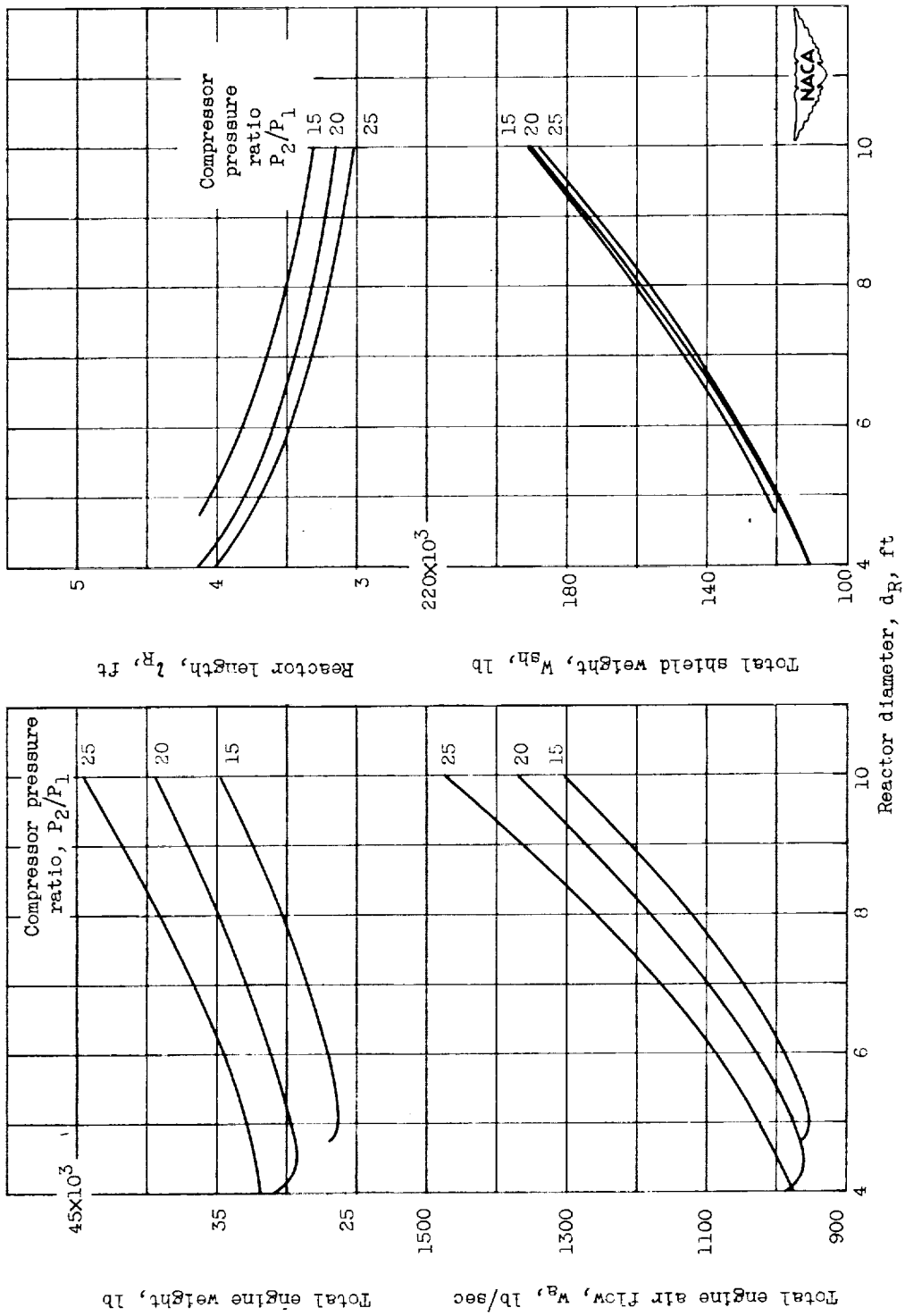

(a) Performance parameters.

Figure 22. - Performance as a function of d_R for several values of P_2/P_1. T_5, 2600° R; α, 0.49. Case III: T_3, 2960° R; ϵ, 0.01 inch.

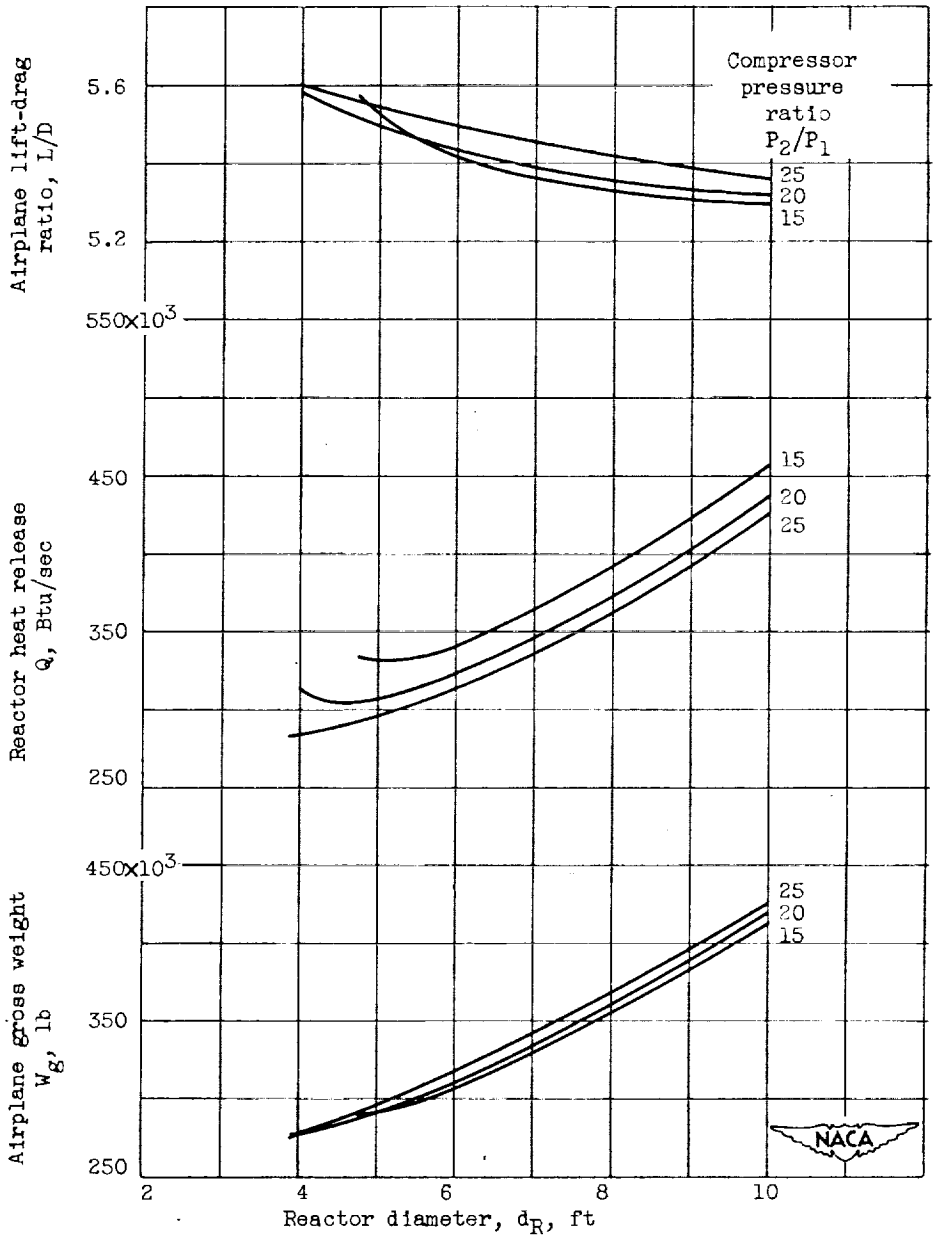

(b) W_g, Q, and airplane L/D.

Figure 22. - Concluded. Performance as a function of d_R for several values of P_2/P_1. T_5, 2600° R; α, 0.49. Case III: T_5, 2960° R; ϵ, 0.01 inch.

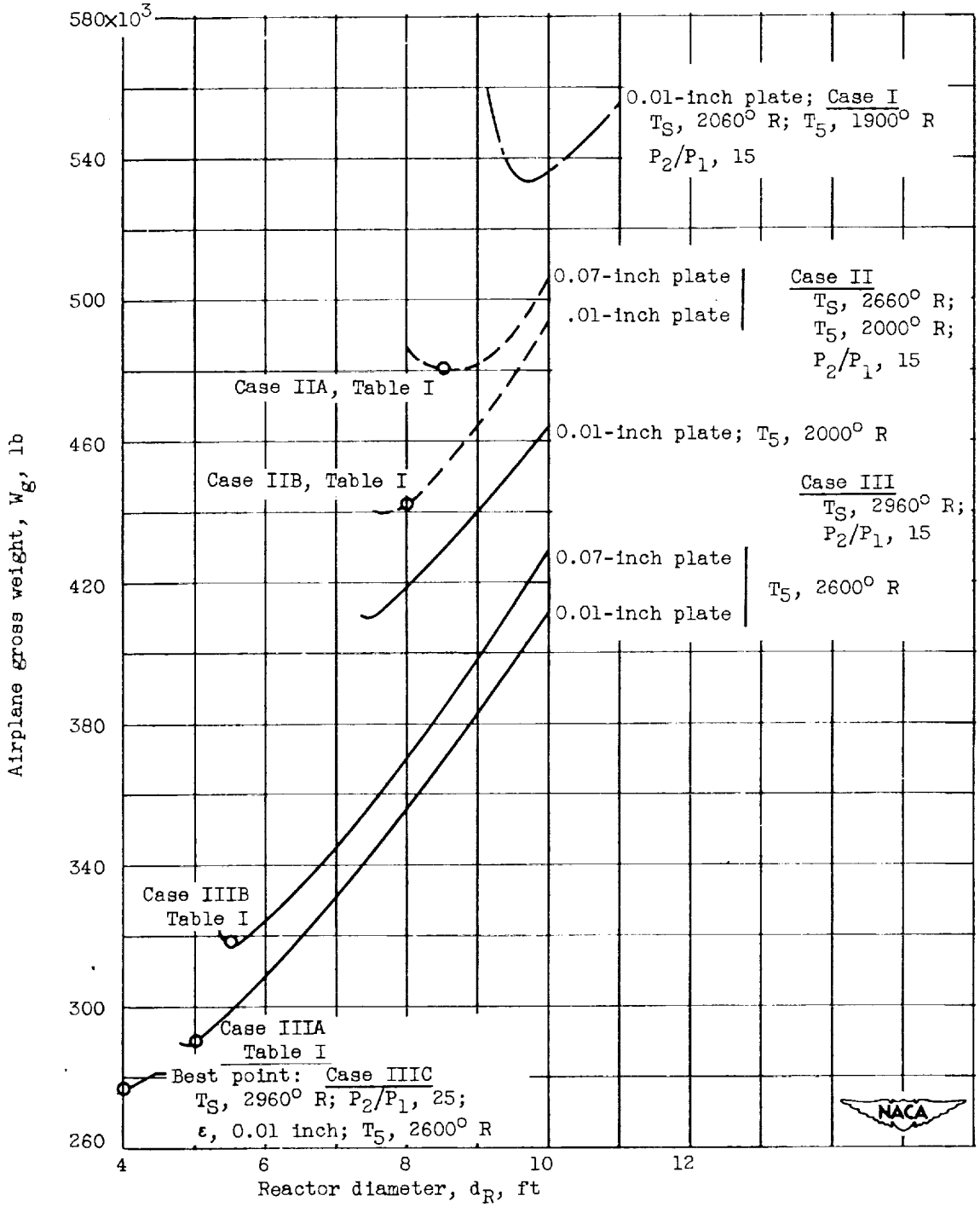

Figure 23. - Comparison curve of cases I, II, and III showing effects of T_S, T_5, ε, and P_2/P_1 on W_g as a function of d_R.

NATIONAL ADVISORY COMMITTEE FOR AERONAUTICS

RESEARCH MEMORANDUM

A DESIGN AND PERFORMANCE STUDY OF THE NUCLEAR DIRECT-AIR-CYCLE SUPERSONIC AIRPLANE, INCLUDING THE EFFECTS OF OPERATING TEMPERATURES AND FUEL PLATE MATERIAL AND THICKNESS

S. V. Manson
Aeronautical Research Scientist

William W. Wachtl
Aeronautical Research Scientist
Propulsion Systems

Approved:

Leroy V. Humble
Aeronautical Research Scientist
Propulsion Systems

Benjamin Pinkel
Chief, Materials and Thermodynamics
Research Division

gah/3-27-53